Electronic Supplementary Material (ESI) for Journal of Materials Chemistry C.

Supporting information for:

Arylene-vinylene Terpyridine Conjugates: Highly Sensitive, Reusable and Simple Fluorescent Probes for the Detection of Nitroaromatics

Amit Sil,[a] Dipanjan Giri,[a] and Sanjib K. Patra*[a]

[a]*Department of Chemistry, Indian Institute of Technology Kharagpur, Kharagpur-721302, WB, INDIA, *E-mail: skpatra@chem.iitkgp.ernet.in; Tel: +913222283338*

1. Materials and methods

All the moisture sensitive reactions and manipulations were carried out under an atmosphere of pre-purified Ar by using standard Schlenk techniques. The glasswares were oven-dried (at 180^{o}C) and cooled under vacuum. Toluene was dried over Na/benzophenone whereas dry methanol and CCl_4 were obtained by distillation over CaH_2. Unless otherwise mentioned all chemicals were of analytical grade, obtained from Aldrich, and used without further purification. Triphenylphosphine (PPh_3) and aryl aldehydes were purchased from Spectrochem. Silica gel (60–120 mesh) used for column chromatography, was purchased from Merck. 2,2′-Azobisisobutyronitrile (AIBN) and PPh_3 were recrystallized from distilled ethanol. Eluting systems for column chromatography purifications were determined by thin layer chromatography (TLC) analysis. TLC plates were visualized under UV light (254 nm/365nm). Solvents were evaporated under reduced pressure using a rotary evaporator.

^{1}H (400 MHz), ^{13}C{^{1}H} (100 MHz), ^{19}F {^{1}H} (376 MHz) and ^{31}P {^{1}H} (162 MHz) NMR spectra were obtained from Bruker Lambda spectrometer using $CDCl_3$ unless otherwise mentioned. Spectra were internally referenced to residual solvent peaks (δ = 7.26 ppm for proton and δ = 77.23 for carbon (middle peak)) in $CDCl_3$. All the coupling constants (*J*) are given in Hz. The HRMS mass spectrometry was recorded in ESI^{+} mode (70 eV) in Waters (Model: Xevo-G2QTOF). The absorption and fluorescence spectra were collected using a Shimadzu (Model UV-2450) spectrophotometer and a Hitachi (Model F-7000) spectrofluorimeter respectively. The time-resolved emission decays were recorded using a time correlated single photon counting (TCSPC) picoseconds spectrophotometer (Model IBH, UK). FTIR spectroscopy was recorded in Spectrum-BX (Perkin Elmer). Spin-Coating was performed in SpinNXG-P1 (Apex). FESEM data was recorded in Supra 40, Carl Zeiss microscope. DLS data was recorded in Malvern Zetasizer Nano equipment. Cyclic voltammetric studies were performed on a BASi Epsilon electrochemical workstation in acetonitrile with 0.1 M tetra-n-butyl ammoniumhexafluorophosphate ($TBAPF_6$) as the supporting electrolyte. The working electrode was a BASi Pt disk electrode, the reference electrode was Ag/AgCl and the auxiliary electrode was a Pt wire. The ferrocene/ferrocenium couple occurs at $E_{1/2}$=+0.51 (70) V versus Ag/AgCl under the same experimental conditions.

2. Synthesis and Characterization

2a. Synthesis

Synthesis of 4′-(4-methylphenyl)-2,2′:6′,2′′-terpyridine (1).

2-Acetyl pyridine (1.8 mL, 16.6 mmol), 4-methylbenzaldehyde (1 mL, 8.3 mmol) and potassium hydroxide (0.93 g, 16.6 mmol) were stirred for 5 min to dissolve in absolute EtOH (40 mL). 35 mL of NH_4OH (25% solution) was added to the reaction mixture and it was allowed to stir at ambient temperature for 24h. The solution turned to orange with formation of product as white precipitate. The precipitate was collected by filtration, and washed sequentially with H_2O and cold MeOH for three times. The white solid was then dried and recrystalized from anhydrous ethanol to afford pure niddle like white crystalline product (1.60 g, 60%).^{1}H NMR ($CDCl_3$, 400 MHz): δ 2.44 (s, 3H, methyl), 7.31 – 7.37 (m, 4H, phenyl), 7.82 (d, J = 8 Hz, 2H, py), 7.88 (m, 2H, py), 8.68 (d, J = 8Hz, 2H, py), 8.73 (d, J = 4 Hz, 2H, py), 8.74 (s, 2H, py); ^{13}C{^{1}H} NMR ($CDCl_3$, 100 MHz): δ 21.5 (methyl), 118.8, 121.6, 123.9, 127.3, 129.8, 135.6, 137.1, 139.3, 149.2, 150.3, 155.9, 156.5.

Synthesis of 4′-(phenyl-*p*-bromomethyl)-2,2′:6′,2′′-terpyridine (2).

An oven-dried 250 mL Schlenk flask that had been thoroughly purged with Ar, was charged with 4’(4-methylphenyl)-2,2’:6’,2’’-terpyridine (5.0 g, 15.5 mmol), NBS (2.9 g, 16.1 mmol) and catalytic amount of AIBN in dry tetrachloromethane (200 mL). The reaction mixture was stirred for 8 h under refluxing condition and then cooled to room temperature. The white precipitate was filtered off and washed with chloroform (20 mL). The organic solution was evaporated under reduced pressure to give white solid product which was purified by recrystallization from anhydrous ethanol. (5.0 gm, 81%). ^{1}H NMR ($CDCl_3$, 400 MHz): δ, 4.57 (s, 2H, methylene), 7.40 (t, J = 8 Hz, 2H), 7.55 (d, J = 8Hz, 2H), 7.93 (m, 4H, py), 8.71 (d, J = 8Hz, 2H, py), 8.75 (d, J = 4 Hz, 2H, py), 8.79 (s, 2H, py); ^{13}C{^{1}H} NMR ($CDCl_3$, 100 MHz): δ 33.2 (methylene), 119.0, 121.6, 124.1, 127.9, 129.8, 137.1, 138.7, 138.8, 149.3, 149.7, 156.1, 156.3.

Synthesis of 4-(2,2′:6′,2′′-terpyridyl-4’)-benzyl triphenylphosphoniumbromide (3).

A mixture of **2** (6.0 g, 18 mmol) and triphenylphosphine (5.89 g, 22.4 mmol) in anhydrous toluene (120 mL) was heated to reflux for 12h. The solution was then allowed to cool to room temperature and off-white precipitate from the resulting solution was filtered off and washed with toluene to remove the excess PPh_3. The product was recrystalized from anhydrous ethanol to give white solid product (9.7 gm, 86%). ^{1}H NMR ($CDCl_3$, 400 MHz): δ 5.62 (d, J = 16 Hz, 2H, methylene), 7.14 –

7.25 (m, 3H), 7.27 – 7.30 (m, 2H), 7.57(d, J = 8Hz, 2H), 7.61 – 7.66 (m, 6H), 7.74 – 7.83 (m, 10H), 8.50 (s, 2H, py), 8.55 (d, J = 8Hz, 2H, py), 8.64 (d, J = 4Hz, 2H, py) ; $^{13}C\{^{1}H\}$ NMR ($CDCl_3$, 100 MHz): δ 30.7 (methylene), 117.6, 118.4, 118.6, 118.8, 121.6, 124.1, 127.7, 128.4, 129.3, 130.3, 132.4,136.7, 135.2, 137.1, 138.5, 149.2, 156.1; ^{31}P $\{^{1}H\}$ ($CDCl_3$, 162 MHz): 23.7 ppm.

Characterization data for P1.

^{1}H NMR ($CDCl_3$, 400 MHz): δ 2.38 (s, 3H, methyl), 7.12 (d, *J* = 16Hz, vinyl 1H), 7.14-7.21 (m, 3H), 7.35-7.37 (m, 2H), 7.45 (d, *J* = 8Hz, 2H), 7.63 (d, *J* = 8 Hz, 2H), 7.86 - 7.94 (m, 4H, py), 8.68 (d, *J* = 8 Hz, 2H, py), 8.76 (d, *J* = 4Hz, 2H, py), 8.78 (s, 2H, py) ; ^{13}C $\{^{1}H\}$ NMR ($CDCl_3$, 100 MHz): δ 21.6 (methyl), 118.8, 121.7, 124.1, 126.8, 127.2, 127.3, 127.8, 129.7, 129.8, 134.7, 137.1, 137.4, 138.1, 138.6, 149.4, 149.9, 156.2, 156.6; HRMS (ESI^+): $C_{30}H_{23}N_3$, Calculated value 426.1970 ($[M+H]^+$); experimental 426.1973 ($[M+H]^+$); FTIR (KBr, cm^{-1}): 2923 ($\bar{\upsilon}_{C\text{-}H\ stretching}$), 1585 ($\bar{\upsilon}_{C=C\ stretching}$), 1566 ($\bar{\upsilon}_{C=N\ stretching}$); $\lambda_{max(\varepsilon)}$: 338 nm (ε = 4.1 × 10^4 $M^{-1}cm^{-1}$), 288 nm (ε = 3.2 × 10^4 $M^{-1}cm^{-1}$); λ_{em}: 423 nm (λ_{ex}: 338 nm).

2b. NMR Spectra

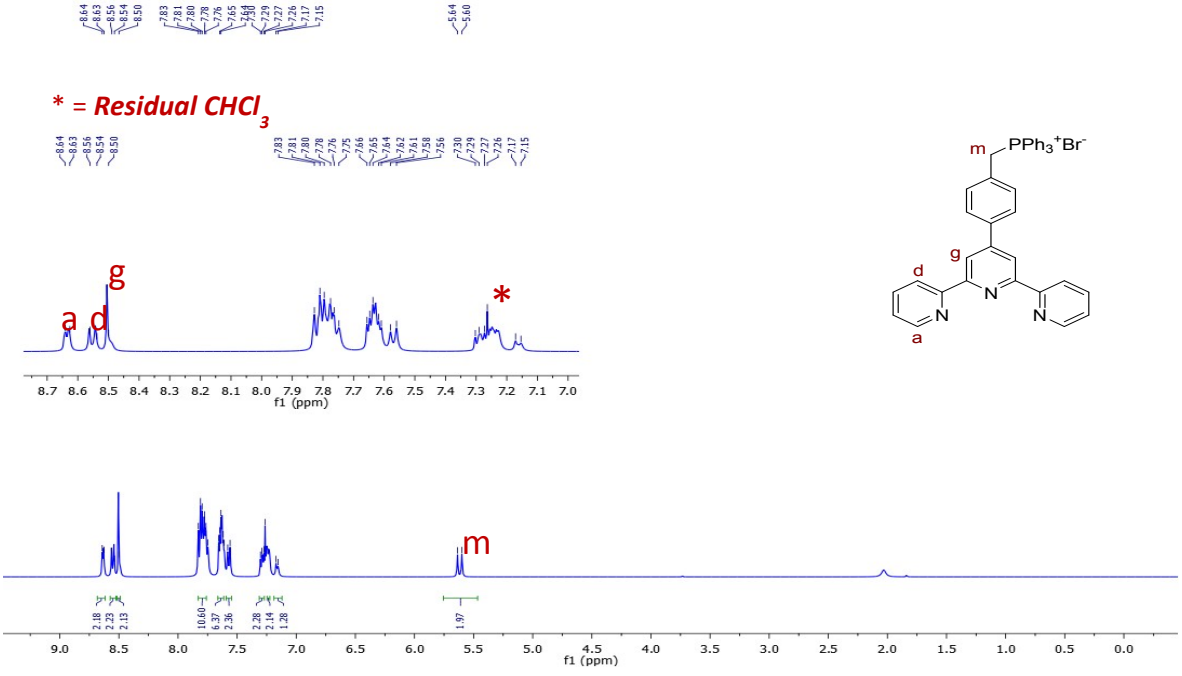

Fig. S1: ^{1}H NMR (400 MHz, $CDCl_3$) spectrum of **3**

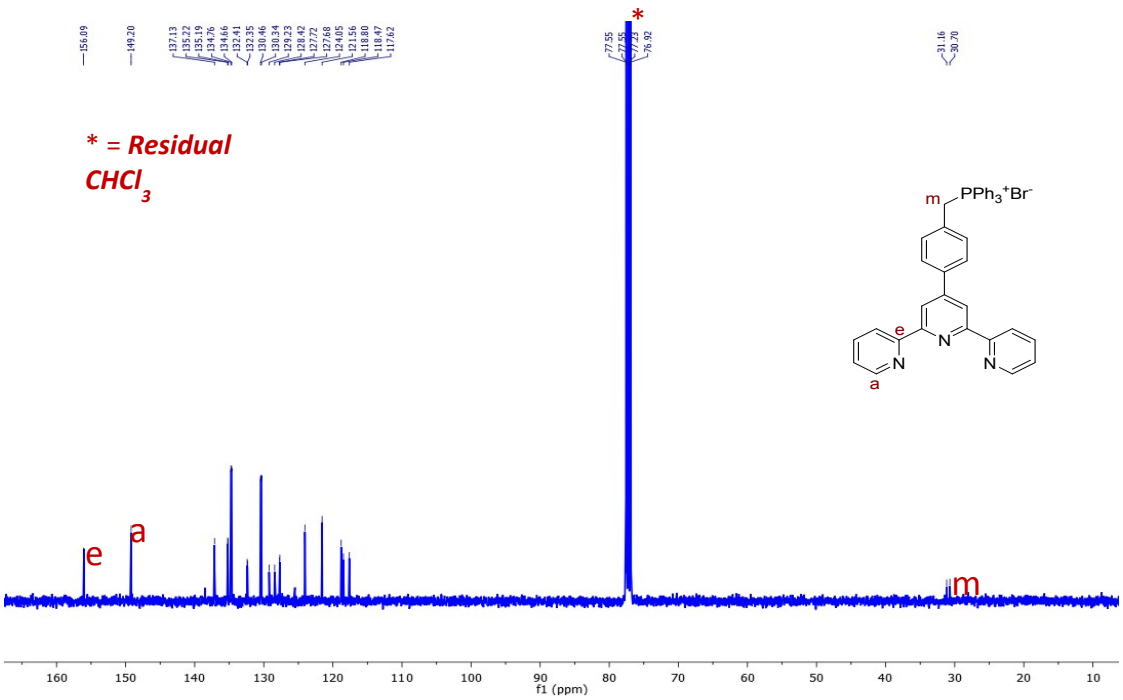

Fig. S2: $^{13}C\{^{1}H\}$ NMR (100 MHz, $CDCl_3$) spectrum of **3**

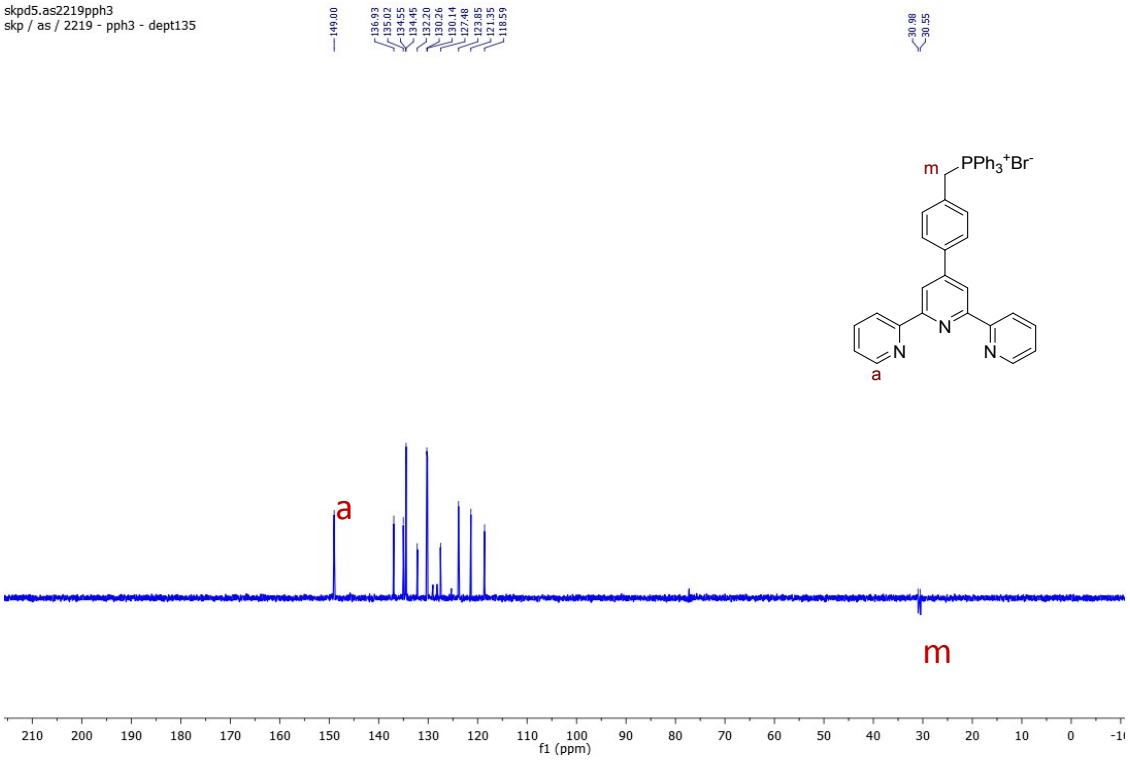

Fig. S3: DEPT-135 NMR (100 MHz, $CDCl_3$) spectrum of **3**

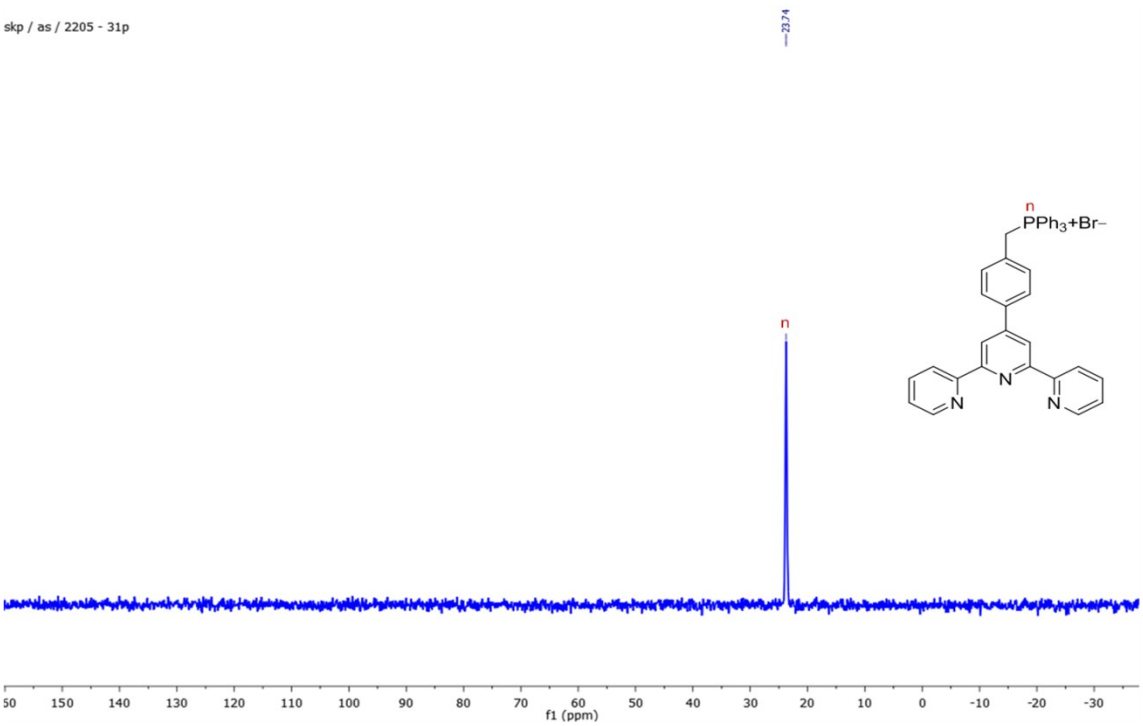

Fig. S4: $^{31}P\{^{1}H\}$ NMR ($CDCl_3$, 162 MHz) spectrum of **3**

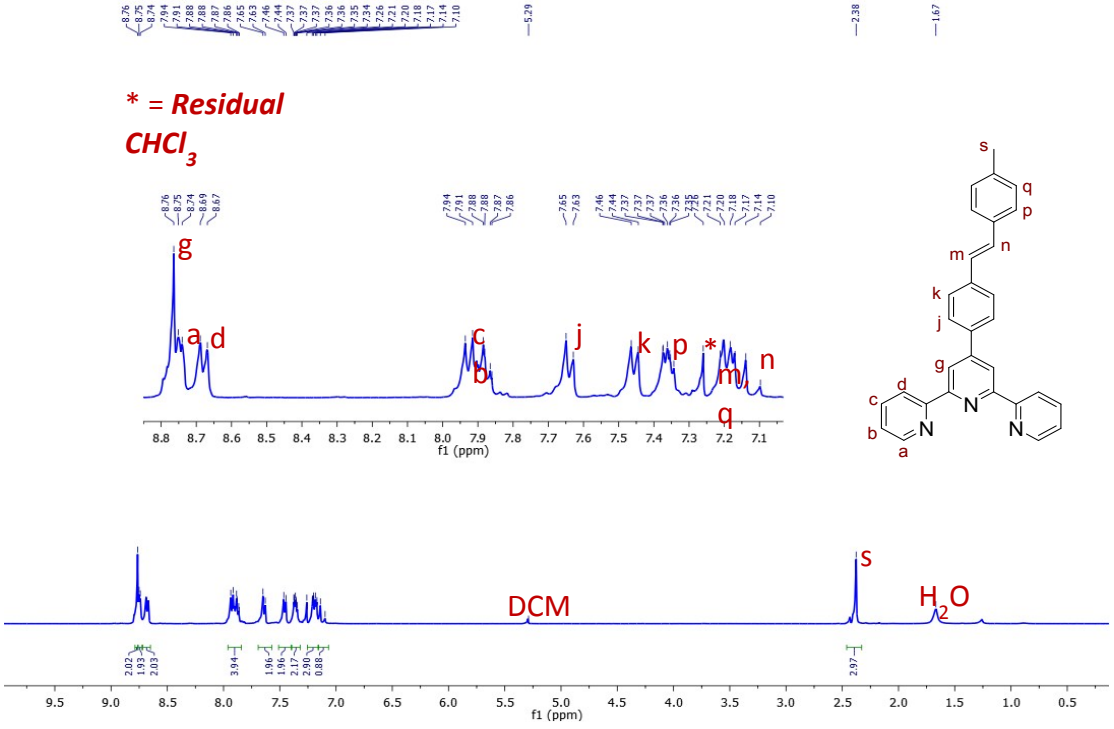

Fig. S5: ^{1}H NMR (400 MHz, $CDCl_3$) spectrum of **P1**; proton marked as q and one of the vinyl protons (m) are overlapped.

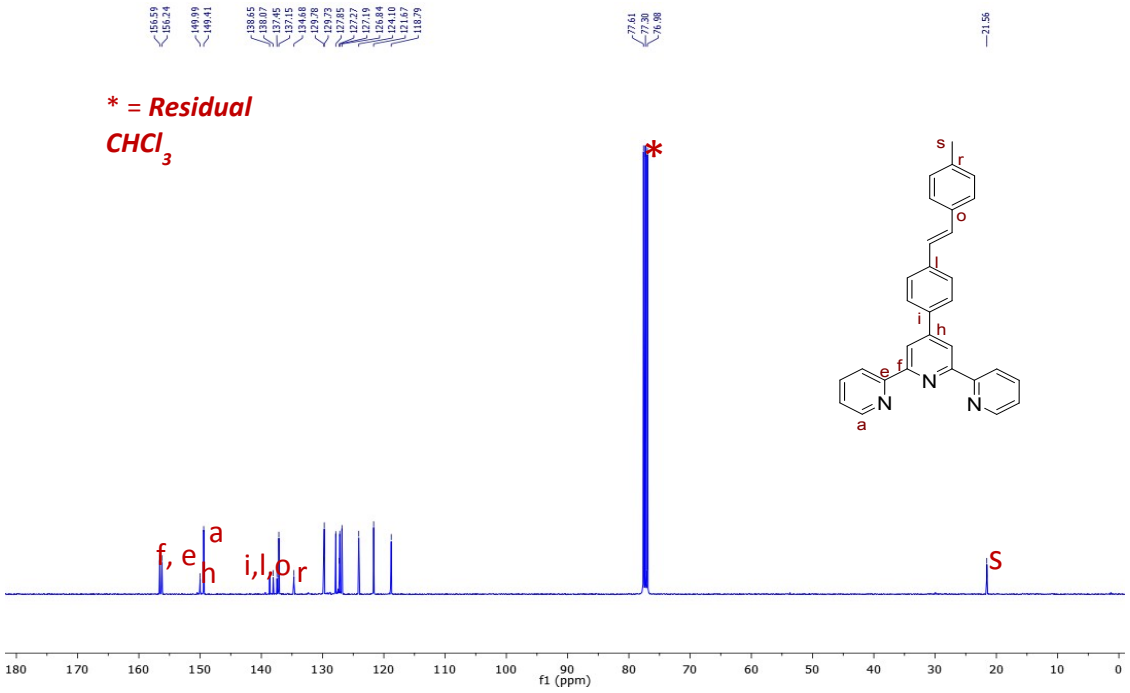

Fig. S6: $^{13}C\{^{1}H\}$ NMR (100 MHz, $CDCl_3$) spectrum of **P1**

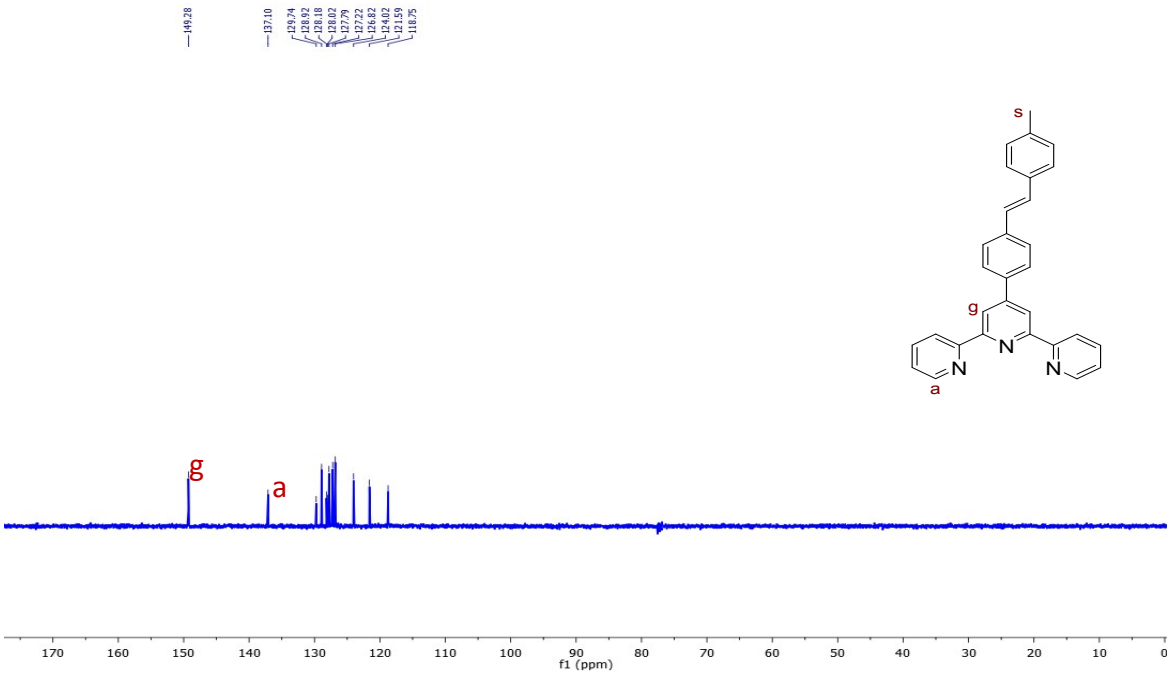

Fig. S7: DEPT-135 NMR (100 MHz, $CDCl_3$) spectrum of **P1**

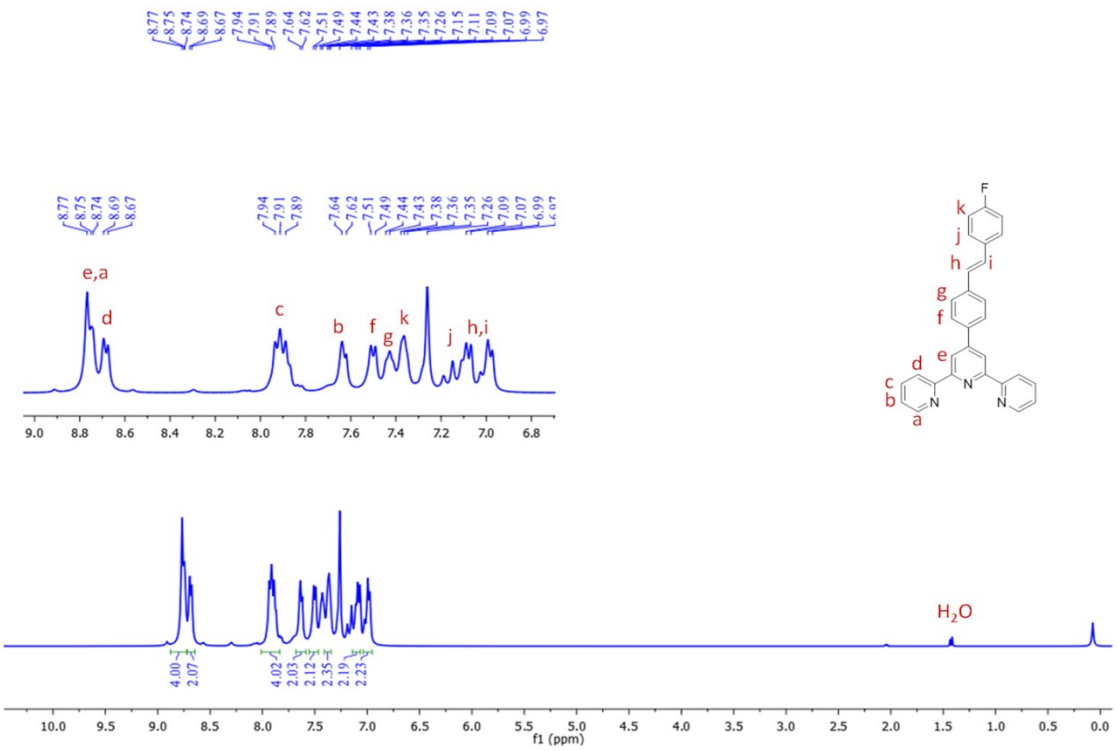

Fig. S8: ^{1}H NMR (400MHz, $CDCl_3$) spectrum of **P2;** proton marked as 'j', 'h' and 'i' are overlapped whereas 'h' and 'i' are the vinylene protons.

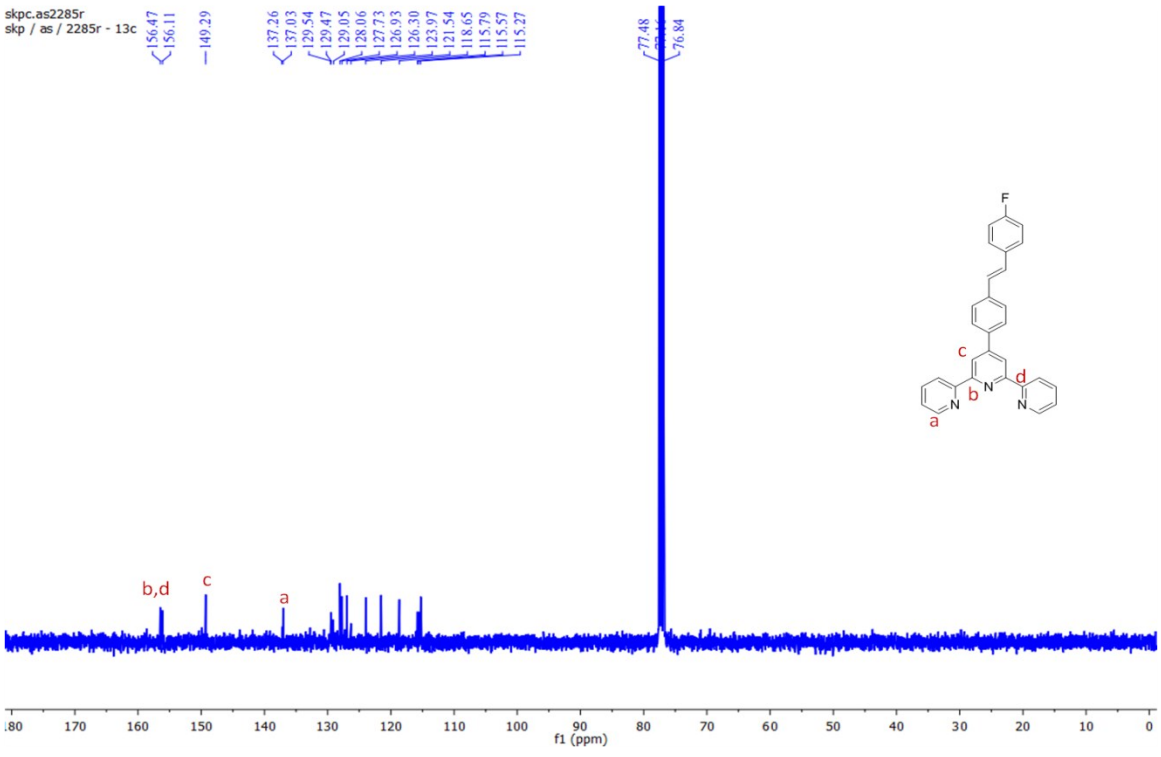

Fig. S9: $^{13}C\{^{1}H\}$NMR (100 MHz, $CDCl_3$) spectrum of **P2**

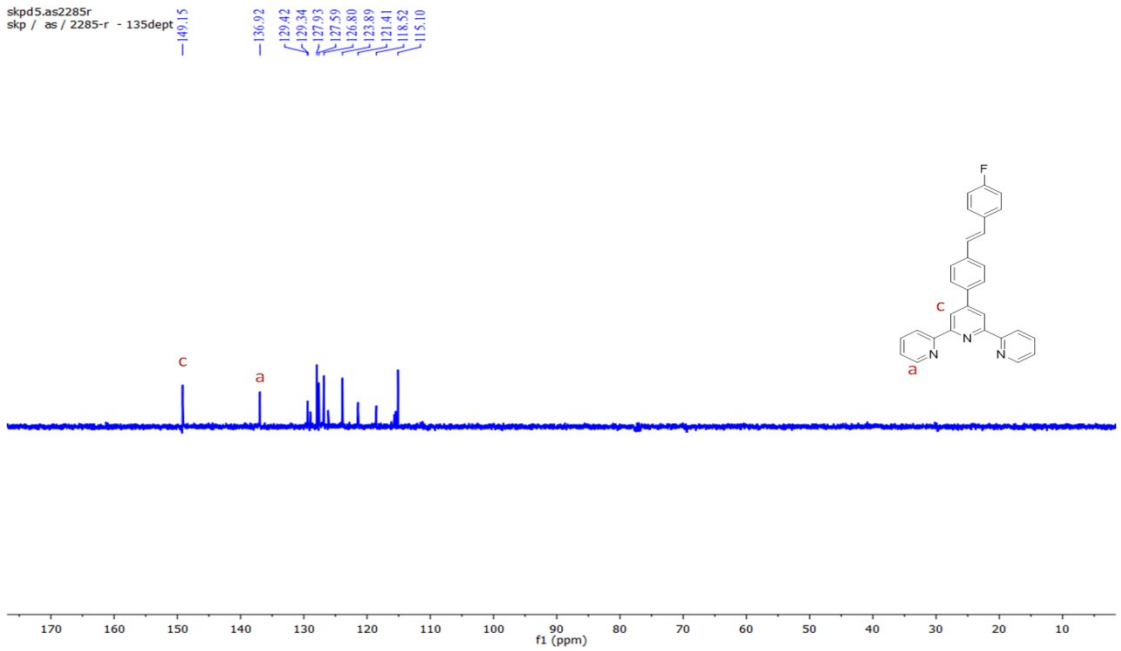

Fig. S10: DEPT-135 NMR (100 MHz, $CDCl_3$) of **P2**

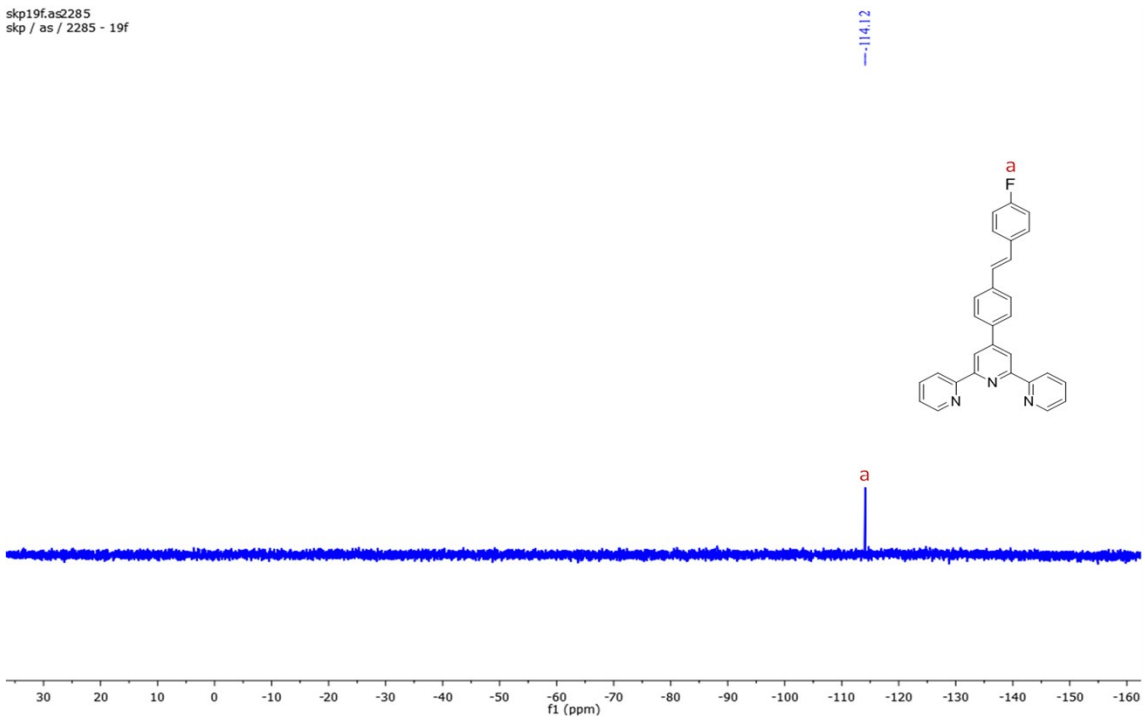

Fig. S11: $^{19}F\{^1H\}$ NMR (376 MHz, $CDCl_3$) spectrum of **P2**

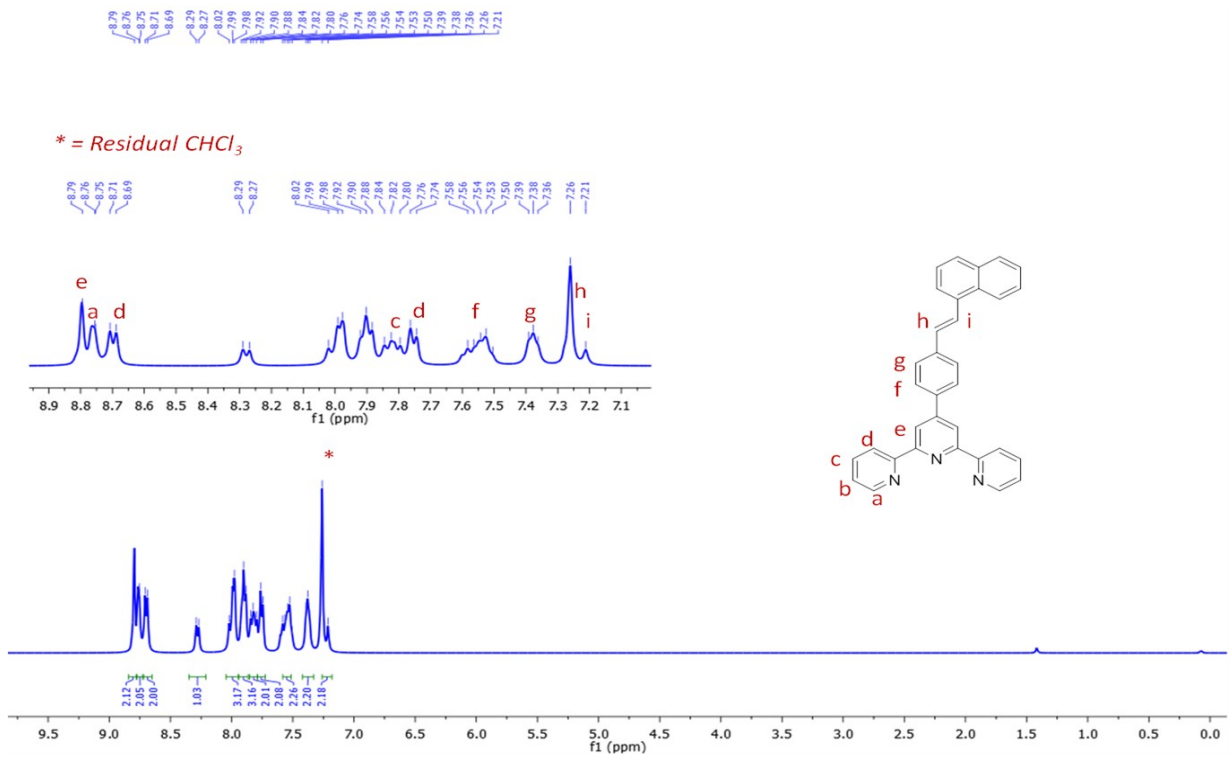

Fig. S12: ^{1}H NMR (400 MHz, $CDCl_3$) spectrum of **P3**; proton marked as 'h' is one of the vinyl protons, which is overlapped with residual $CHCl_3$.

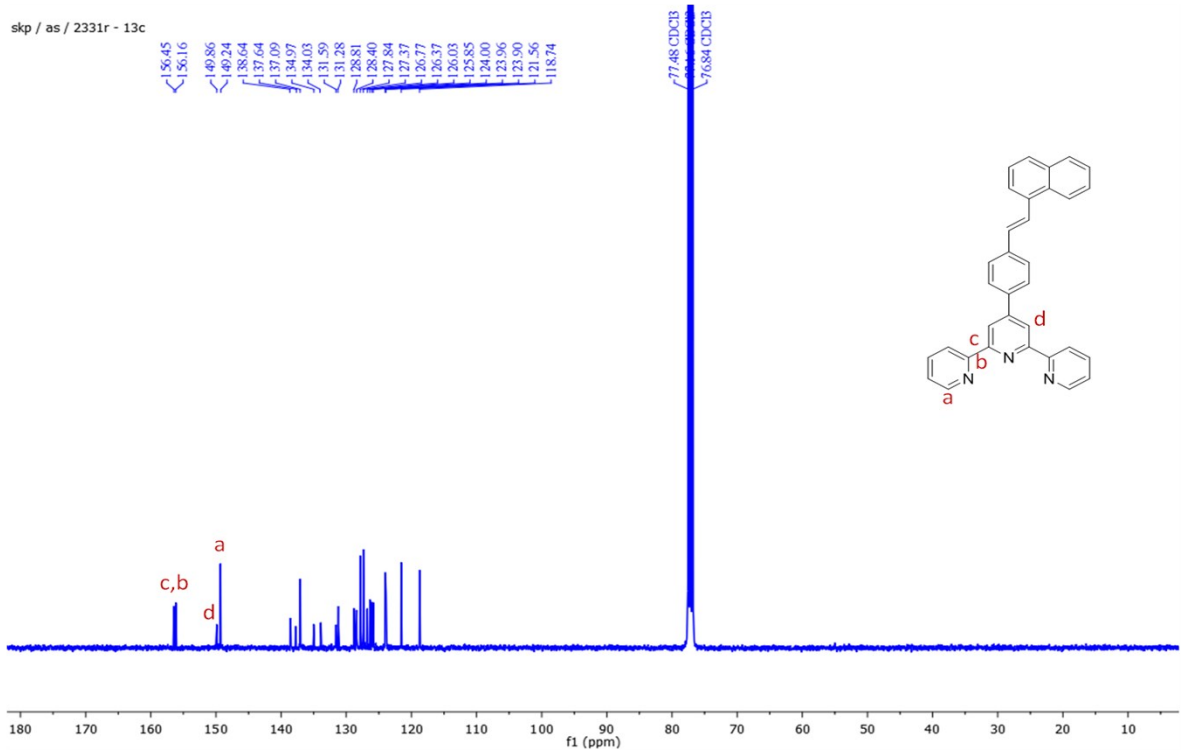

Fig. S13: $^{13}C\{^{1}H\}$NMR (100 MHz, $CDCl_3$) spectrum of **P3**

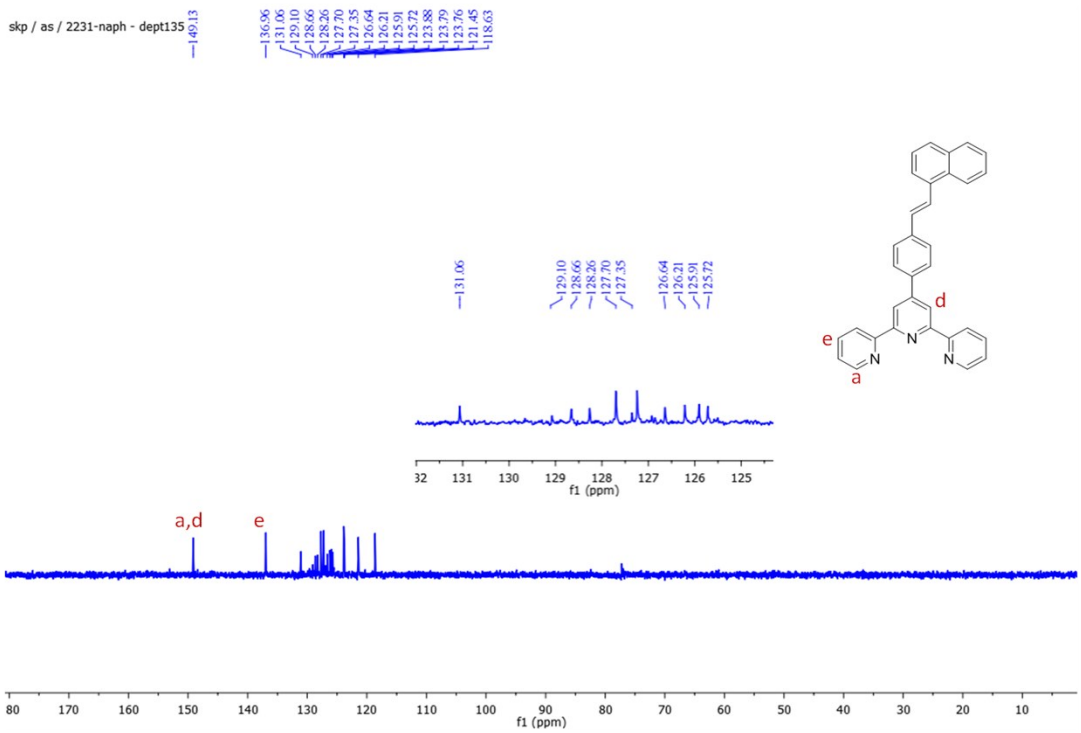

Fig. S14: DEPT-135 NMR (100 MHz, $CDCl_3$) spectrum of **P3**

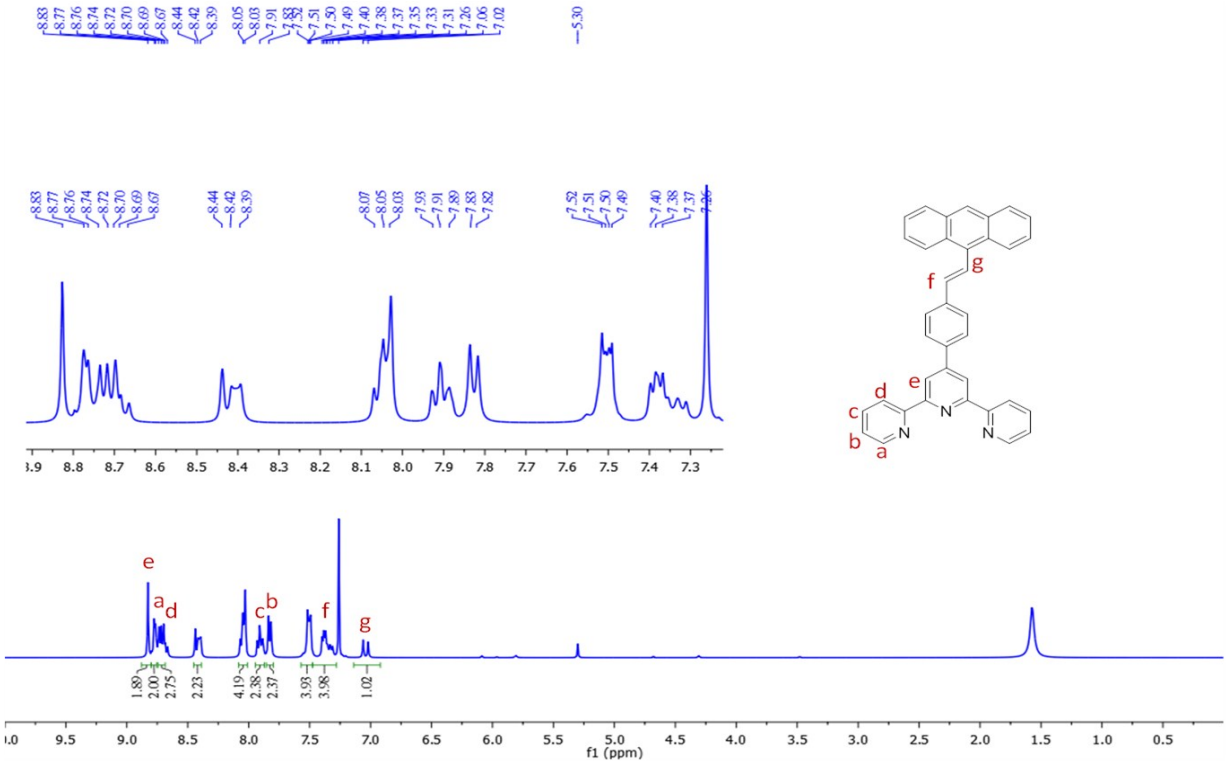

Fig. S15: ^1H NMR (400 MHz, $CDCl_3$) spectrum of **P4**; proton marked as f is one of the vinyl proton which is overlapped with other aromatic protons.

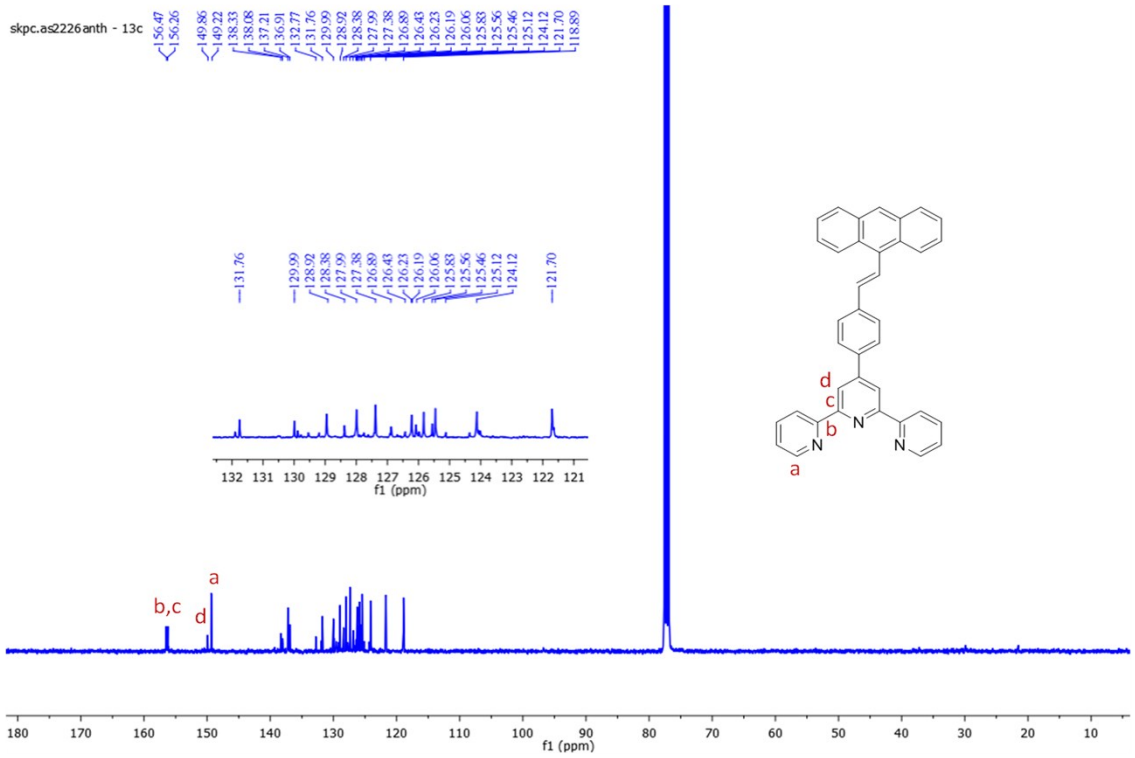

Fig. S16: $^{13}C\{^{1}H\}$ NMR (100 MHz, $CDCl_3$) spectrum of **P4**

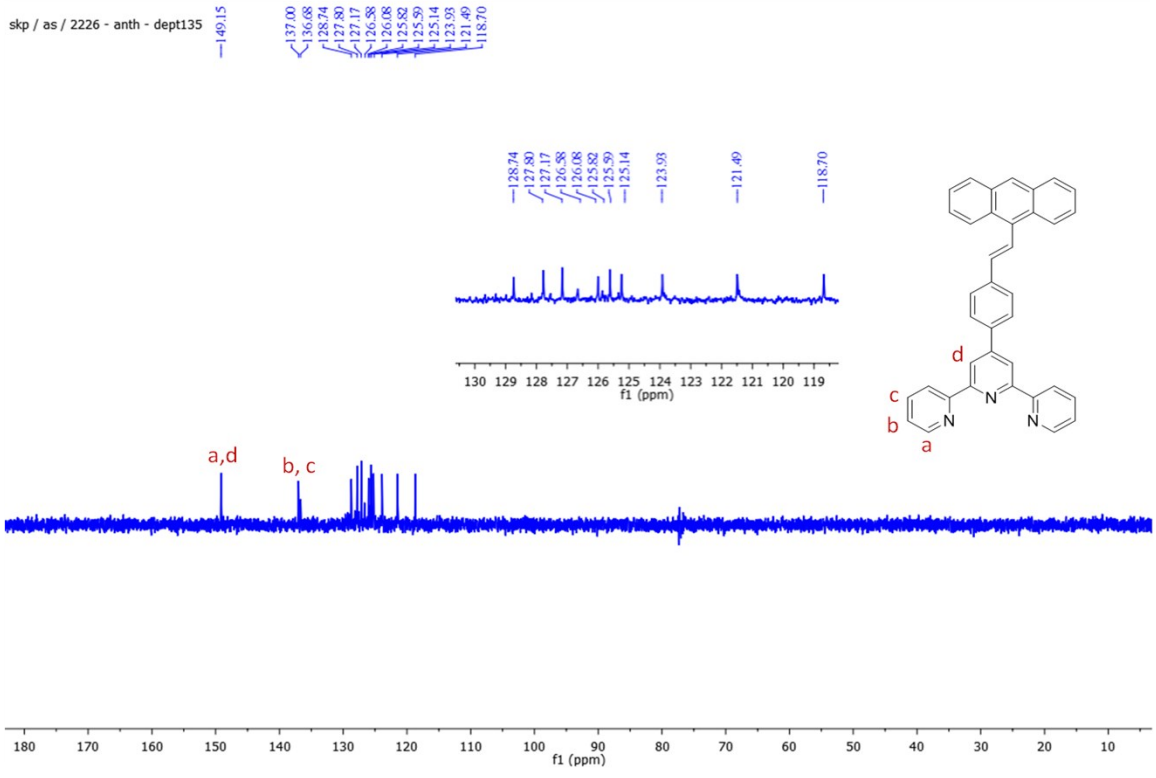

Fig. S17: DEPT-135 NMR (100 MHz, $CDCl_3$) spectrum of **P4**

2c. FTIR data (measured as KBr pellets)

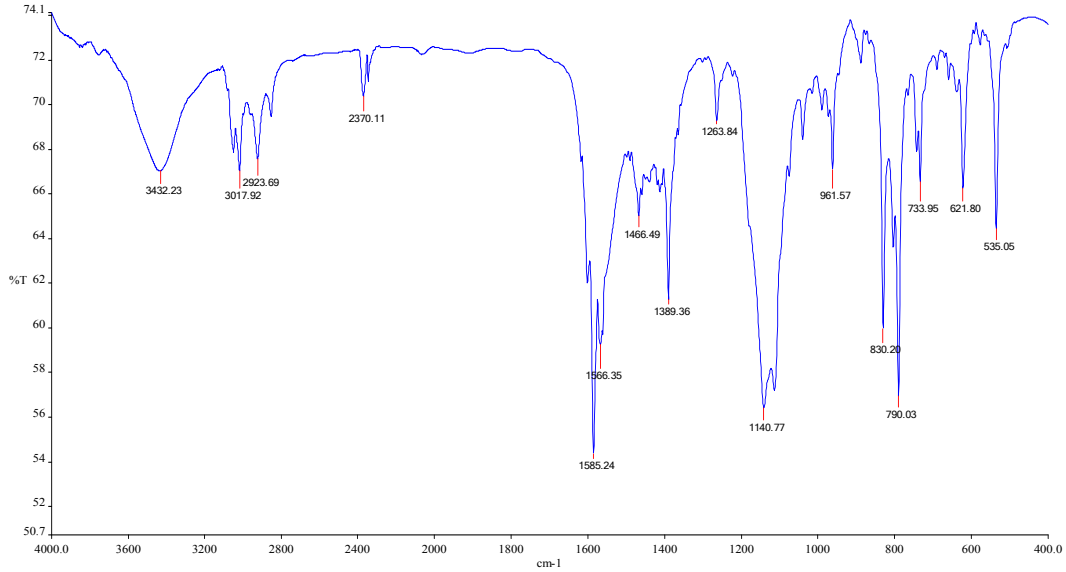

Fig. S18: FTIR spectrum of **P1**

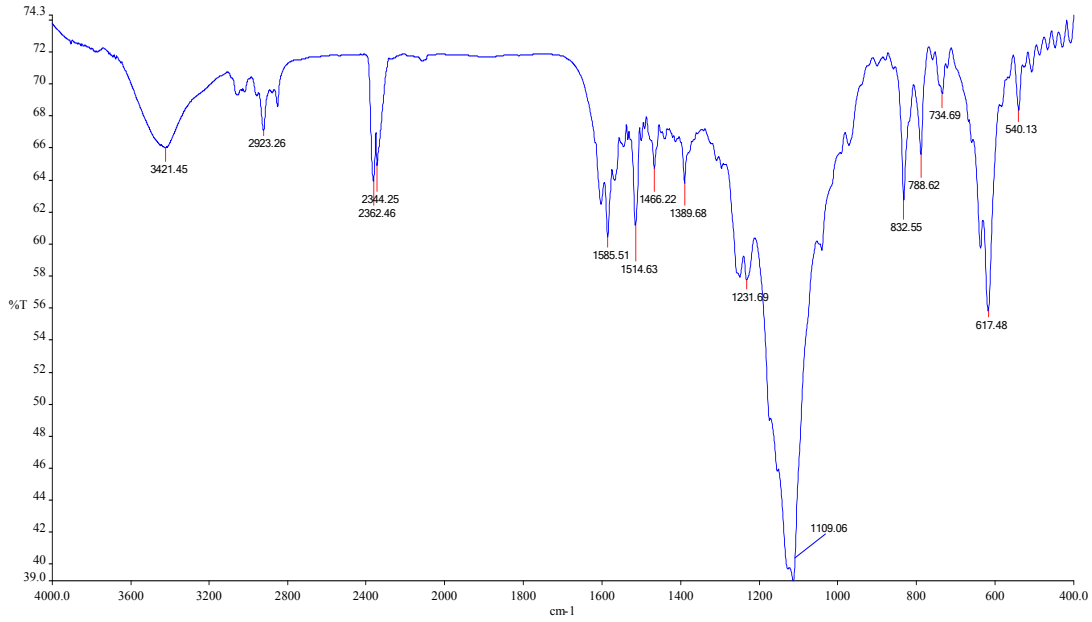

Fig. S19: FTIR spectrum of **P2**

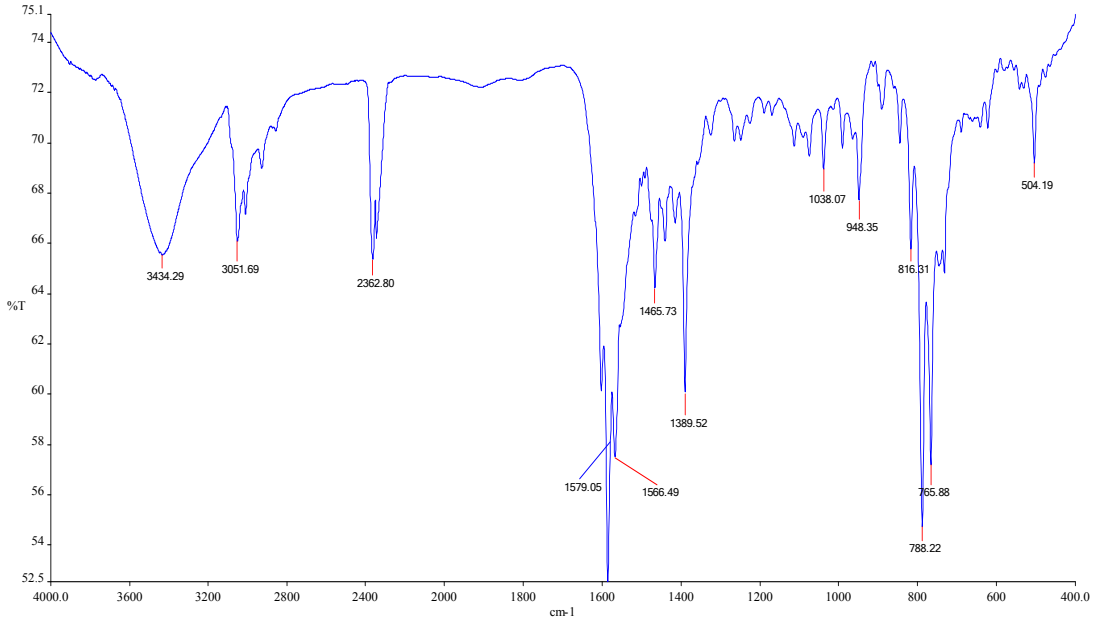

Fig. S20: FTIR spectrum of **P3**

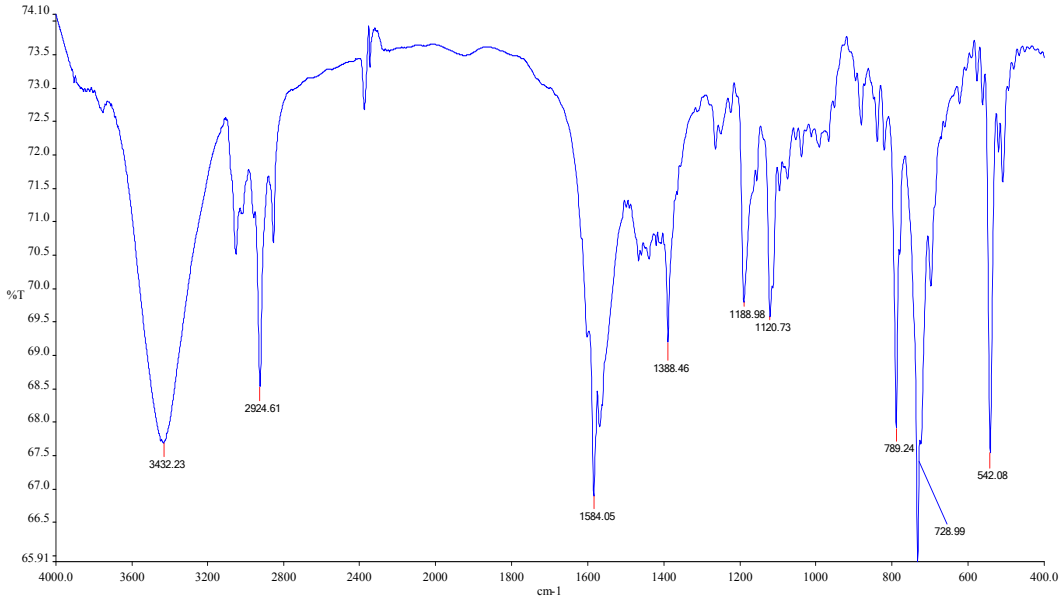

Fig. S21: FTIR spectrum of **P4**

2d. Mass spectrometry data

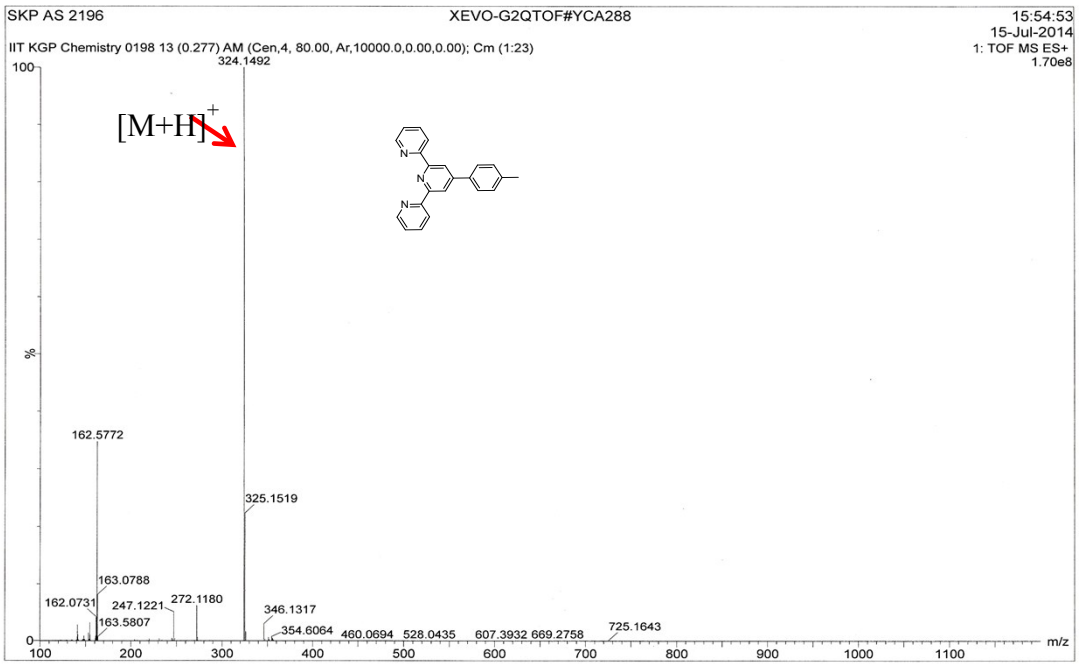

Fig. S22: HRMS (ESI$^+$) of **1**

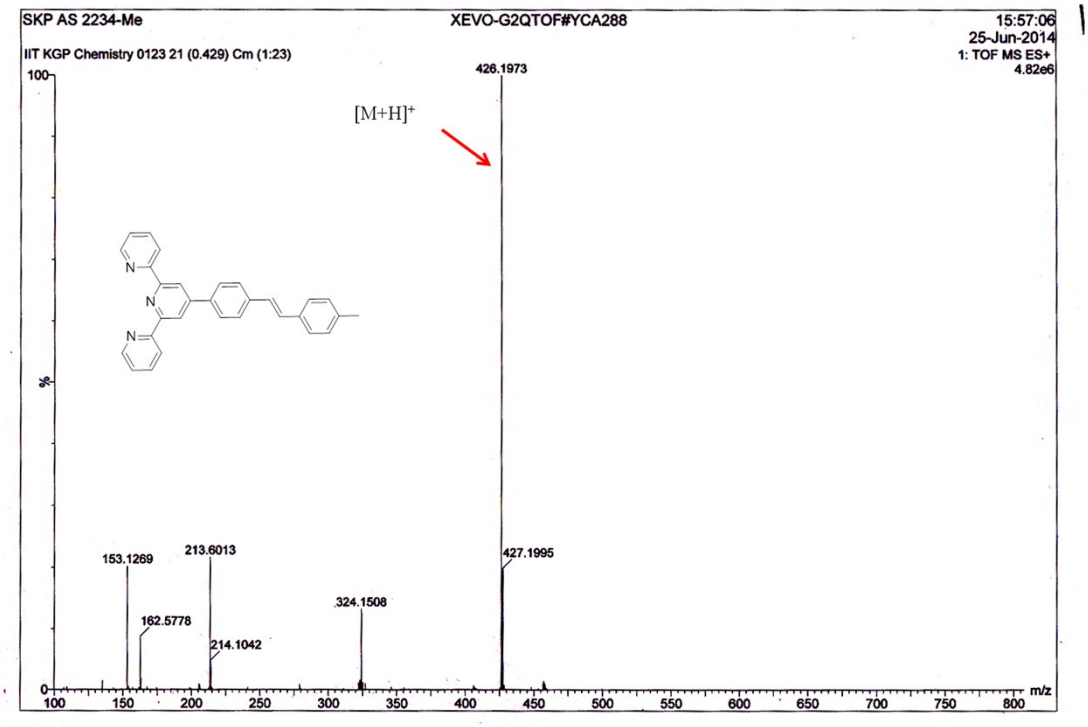

Fig. S23: HRMS (ESI$^+$) of **P1**

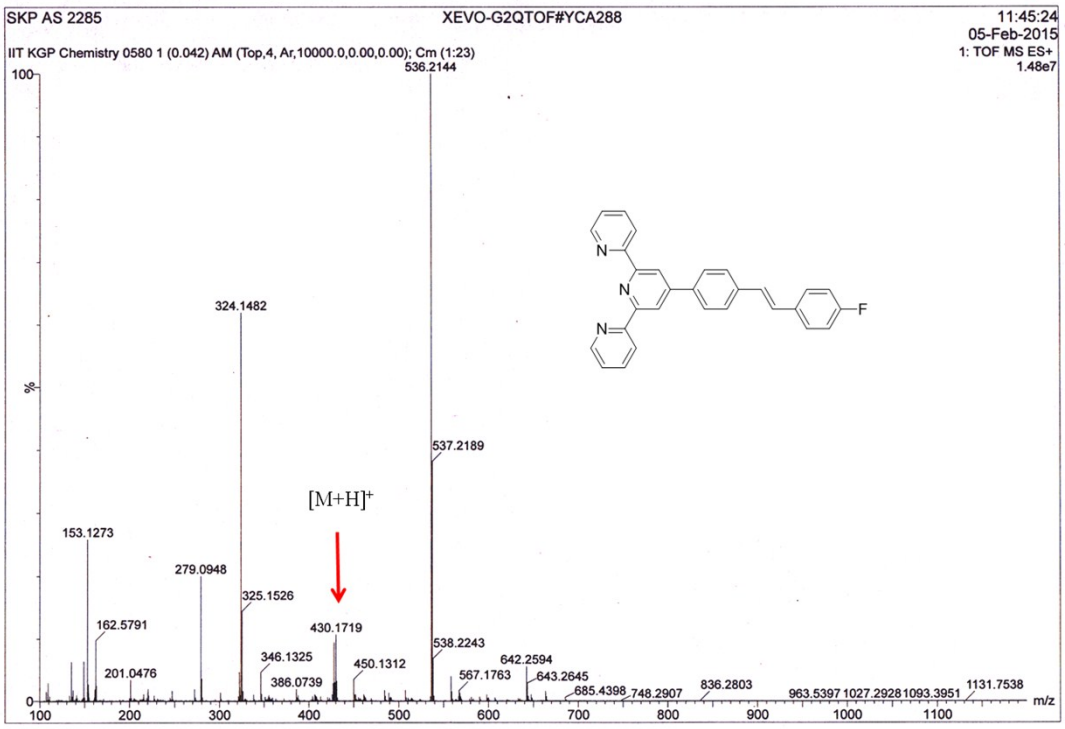

Fig. S24: HRMS (ESI$^+$) of **P2**

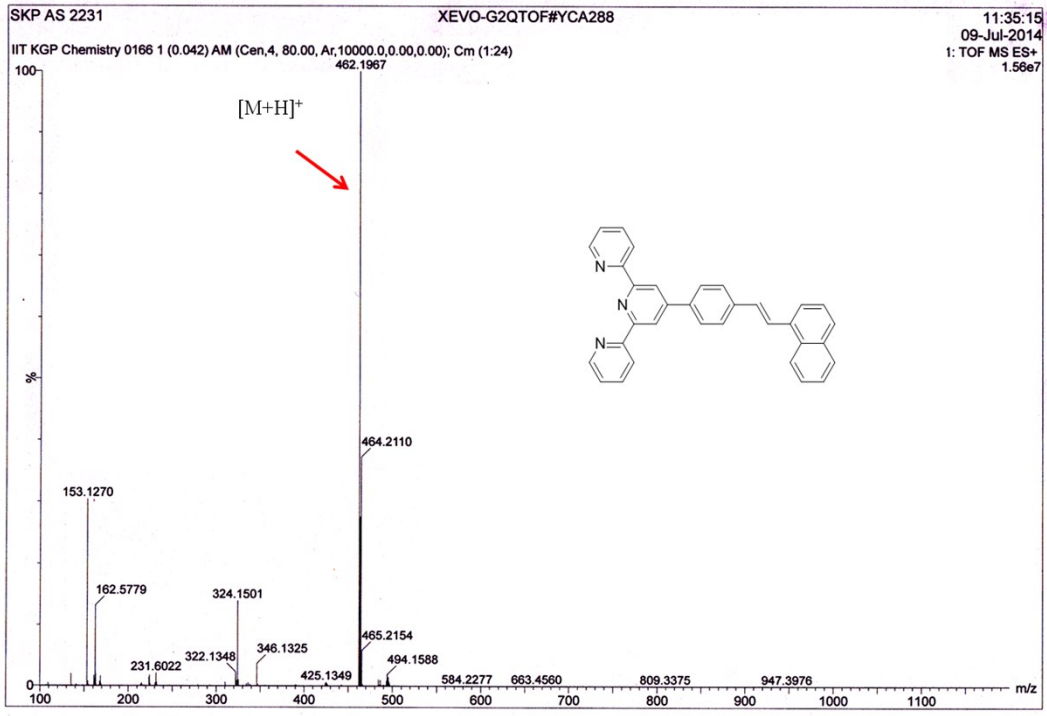

Fig. S25: HRMS (ESI$^+$) of **P3**

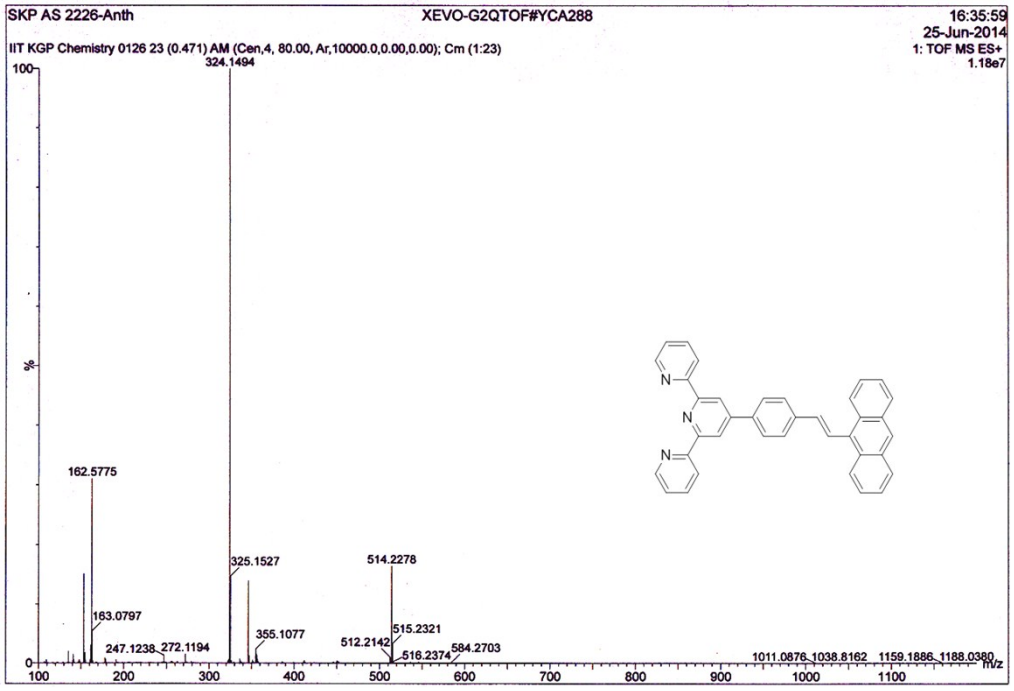

Fig. S26: HRMS (ESI$^+$) of **P4** (Interestingly, a peak was observed at 514.4276 corresponding to ([M+3H]$^+$) instead of 512.2126 for ([M+H]$^+$). However in LCMS study, the peak for ([M+H]$^+$) was observed as shown below.

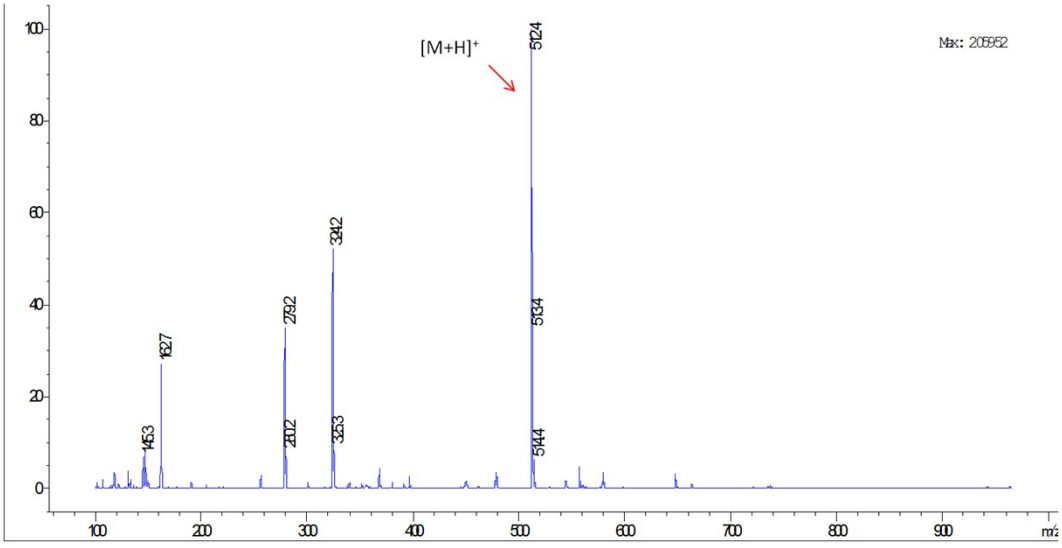

Fig. S27: LCMS (ESI$^+$) of **P4** (LCMS study was carried out by a single quadruple mass analyzer

3. Photophysical and Sensing Studies

3a. Determination of Quantum yield

All the UV−Vis absorption and emission spectra were recorded using a Shimadzu UV−Vis spectrophotometer (model UV 2450 and a Spex Fluorolog-3 spectrofluorimeter (model FL3−11) respectively. The concentration of the probe was maintained at 10^{-5} M. Fluorescence quantum yields were measured with respect to a secondary standard quinine sulphate (λ_{abs} = 350 nm) in 0.1 M H_2SO_4 (Φ = 0.54) at 298 K, following the equation.[1]

$$\frac{\Phi_S}{\Phi_R} = \frac{A_S}{A_R} \times \frac{(Abs)_R}{(Abs)_S} \times \frac{\eta_S^2}{\eta_R^2}$$

Here Φ represents the quantum yield, (Abs) represents the absorbance, A represents the area under the fluorescence curve, and η is the refractive index of the medium. The subscript S and R denote the corresponding parameters for the sample and reference respectively.

3b. Determination of time resolved fluorescence spectra

The time-resolved emission decays were recorded using a time correlated single photon counting (TCSPC) picoseconds spectrophotometer. **P1**, **P2** and **P3** were excited using a picosecond diode laser at 340 nm (IBH, UK, Nanoled) whereas **P4** was excited at 400 nm using the same laser. The signals were recorded at magic angle (54.71) using a Hamamatsu microchannel plate photomultiplier tube (3809U). The typical instrument response functions in our setup are 100 ps (for **P4**) and ~800 ps (for **P1**-**P3**). Time-resolved fluorescence decays were analyzed using IBH DAS-6 decay analysis software. The radiative and non-radiative decay constants were calculated from the equations, $k_r = \Phi/\tau$ and $k_{nr} = (1-\Phi)/\tau$, where Φ = quantum yield and τ= lifetime and were tabulated in Table S1.

Table S1: Time resolved fluorescence data of **P1**-**P4**

Probes	$\langle\tau\rangle^a$***/ns***	$k_{nr}(s^{-1})/10^{10}$	$k_r(s^{-1})/10^{10}$
P1	1.36	5.6	1.69
P2	0.94	8.0	2.55
P3	1.91	3.5	1.67
P4	2.88	2.2	1.25

[a]Error limit =± 5%

3c. Solid state absorption and emission spectra of the probes

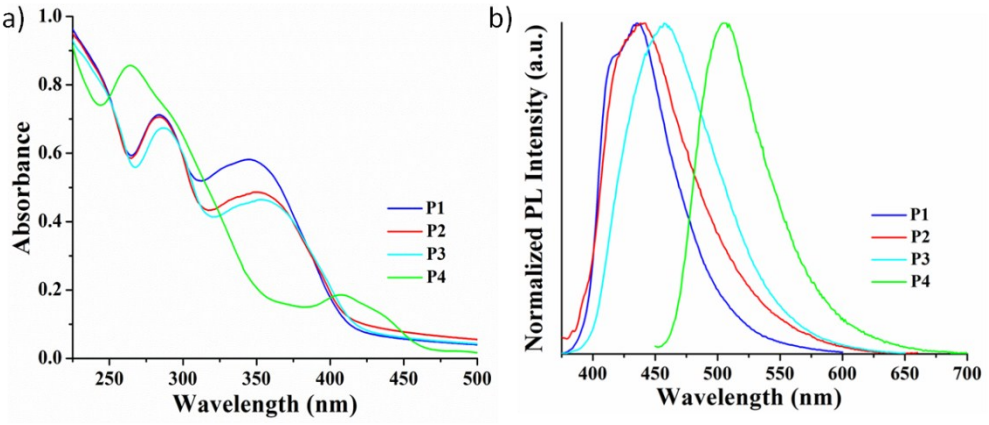

Fig. S28: Solid state (a) absorption and (b) emission spectra of **P1-P4** at ambient temperature. The optical energy band gap (E_g^{opt}) of the probes was calculated by inspecting the edge of the solid state absorption spectra by using the equation $E_g^{opt}(eV) = 1240/\lambda_{cut\ off}$.

Table S2: Absorption and emission spectral Data of P1 - P4 in solid state

Probes	Absorption (nm)	Emission (nm)	[a]Stokes Shift (cm^{-1})
P1	346, 284	435,415 (sh)	5913
P2	354,285	440	5521
P3	357, 286	458	6177
P4	408, 263	504	4668

[a]Stokes shifts $\Delta\lambda_{st}$, $cm^{-1} = \lambda_{em} - \lambda_{abs}$.

3d. Concentration dependent fluorescence study

To determine the optimum concentration in which self-aggregation of the sensing probe in solution is less, the concentration dependent emission spectra (1×10^{-3} M to 1×10^{-5} M) was recorded in $CHCl_3$. All the arylene-vinylene conjugated terpyridines displayed less aggregation behavior with concentration 10^{-5} M as evidenced from concentration-dependent fluorescence study.

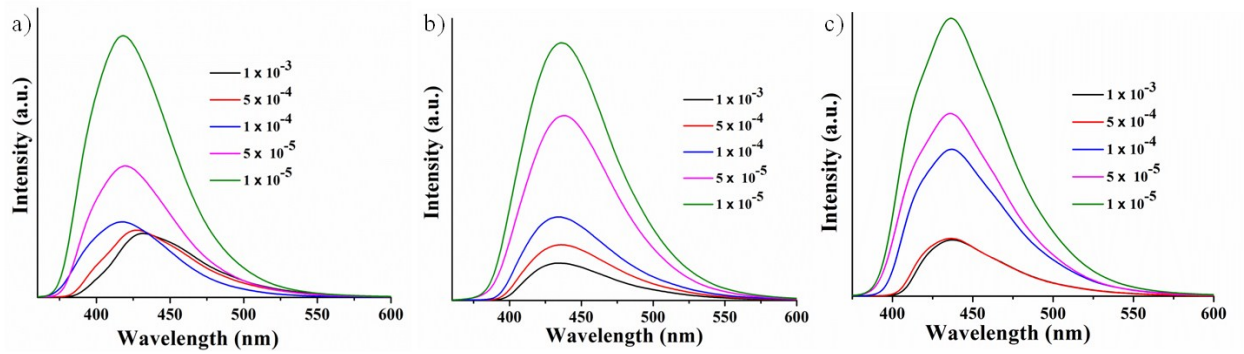

Fig. S29: Concentration dependent fluorescence spectra of (a) **P1**, (b) **P2** and (c) **P3** in $CHCl_3$ at ambient temperature.

3e. Particle size measurement by DLS

The particle size of the probes was measured by dynamic light scattering (DLS) experiment to confirm the aggregate formation in solution. The particle size of all the probes were measured in $CHCl_3$ by varying the concentration ranging from 10^{-3} to 10^{-5} M and different particle sizes were found.

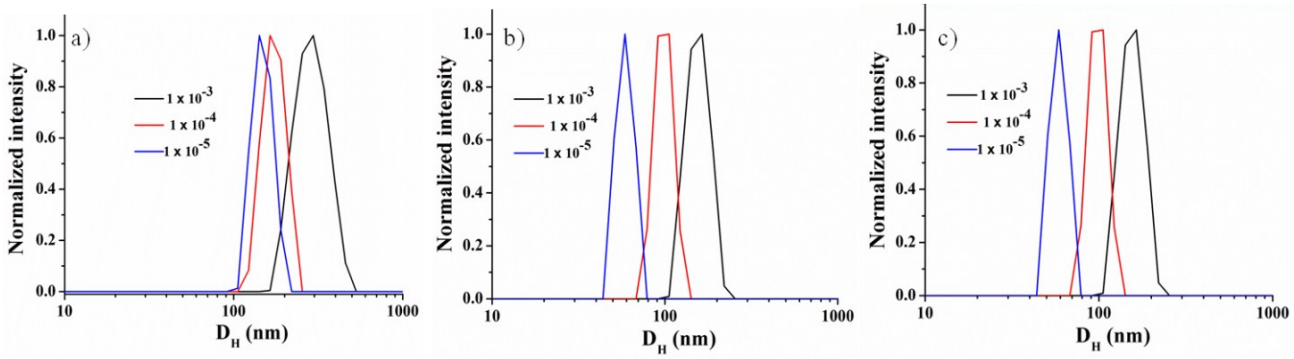

Fig. S30: Concentration dependent DLS spectra of (a) **P1**, (b) **P2** and (c) **P3** in $CHCl_3$ solution at ambient temperature.

3f. Fluorescence titration studies of the sensing probes towards PA

The fluorescence spectroscopic titrations were performed with a continuous variation of concentrations (~1 x 10^{-5} M to ~1 × 10^{-3} M) of PA in $CHCl_3$.

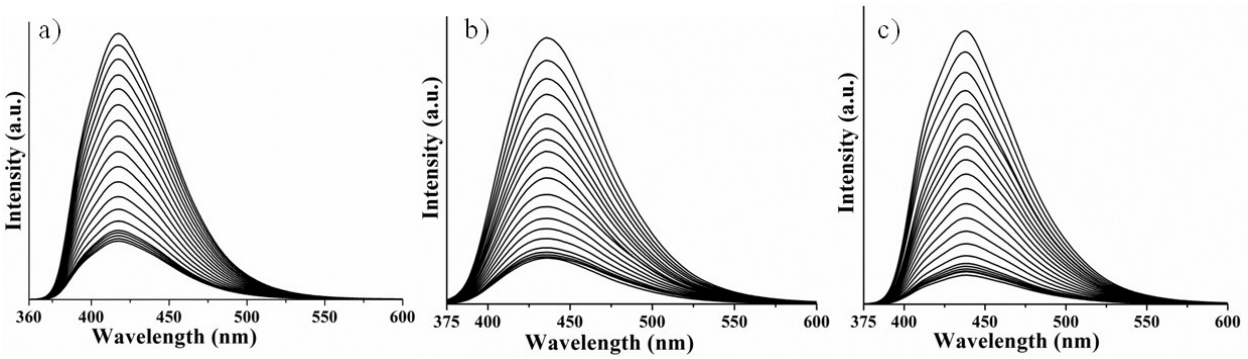

Fig. S31: Fluorescence quenching behaviour of (a) **P1**, (b) **P2** and (c) **P3** upon incremental addition of PA.

3g. Fluorescence response of the sensing probes towards TFA

2 µL of Strong non-aromatic acid (trifluoro acetic acid) was added to the probe solution (1×10^{-5} M in $CHCl_3$) under the same set of condition as used for PA and the corresponding fluorescence data was recorded to confirm the possibility of excited state proton transfer.

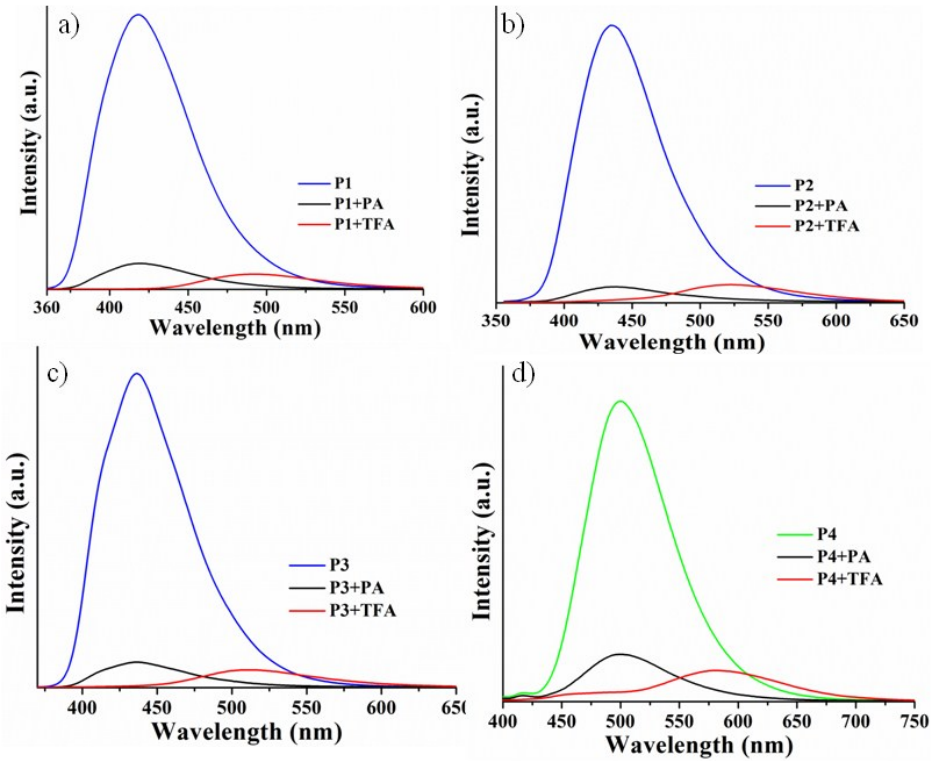

Fig. S32: Fluorescence spectra of (a) **P1**, (b) **P2**, (c) **P3** and (d) **P4** upon addition of picric acid and trifluoroacetic acid.

3h. Spectral overlap between absorption and emission spectra of the probes.

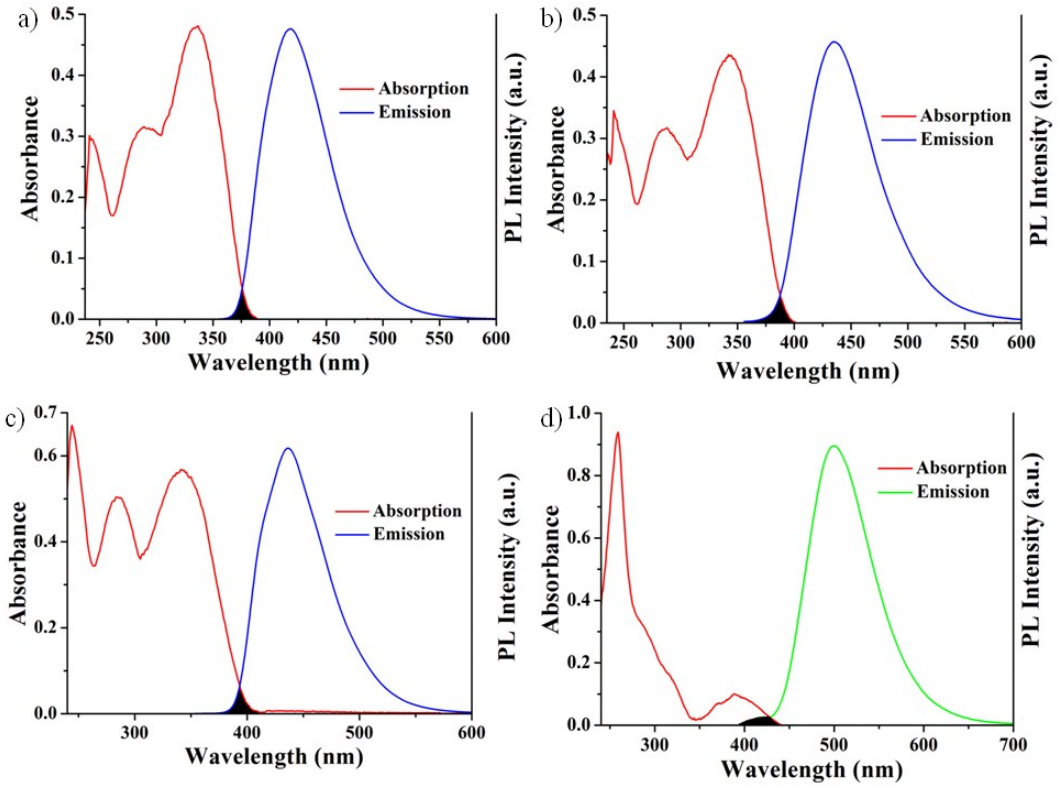

Fig. S33: Absorption and emission spectra of (a) **P1**, (b) **P2**, (c) **P3** and (d) **P4** in $CHCl_3$ (1×10^{-5} M) at ambient temperature.

3i. Calculation of Stern–Volmer constants:

The sensitivity of the sensing probes (**P1- P4)** towards the nitroaromatics was estimated from their Stern–Volmer constants, K_{sv} as determined from the equation:

$$I_o/I = 1 + K_{sv}[Q]$$

Where, I_o and I are the fluorescence intensities in the absence and presence of nitroaromatics respectively, and the Stern– Volmer plots were plotted as a function of the nitroaromatic concentration, [Q]. The Stern–Volmer constants, K_{sv} can be calculated from the slope of the Stern–Volmer plots.

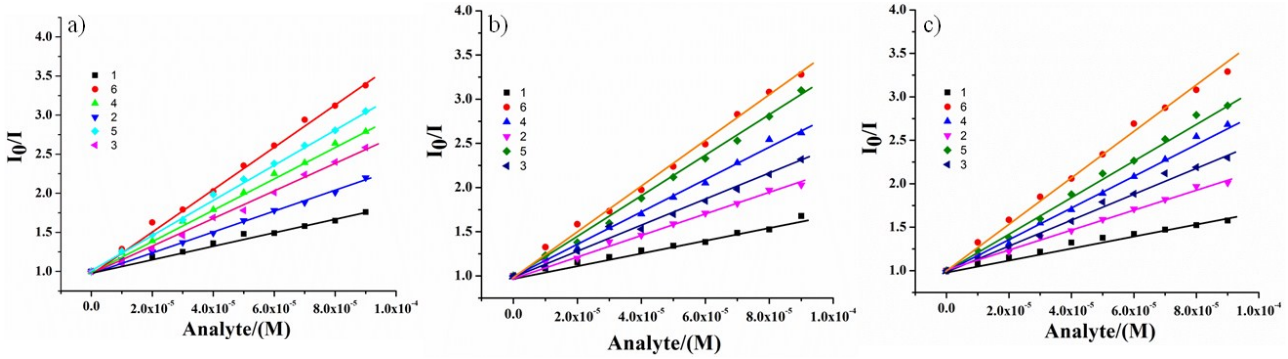

Fig. S34: The Stern-Volmer plot for (a) **P1**, (b) **P2** and (c) **P3** towards the different NACs. 1: NB, 2: NT, 3: HNB, 4: NBA, 5: DNT, 6: PA.

3j. Calculation of the Limit of Detection (LOD):

The limit of detection (LOD) of the sensing probes **(P1-P4)** was determined from emission spectra using the following equation:

DL = 3σ/S where, σ standard deviation of the blank solution; S is the slope of the between fluorescence intensity and picric acid concentration.

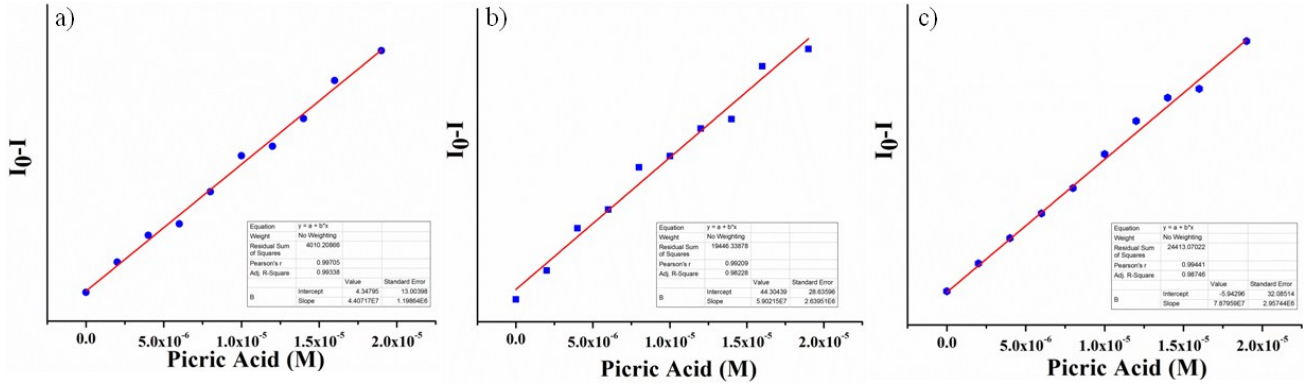

Fig. S35: The limit of detection (LOD) plot for (a) **P1**, (b) **P2** and (c) **P3** towards picric acid.

3k. Time resolved fluorescence spectra of the sensing probes towards PA

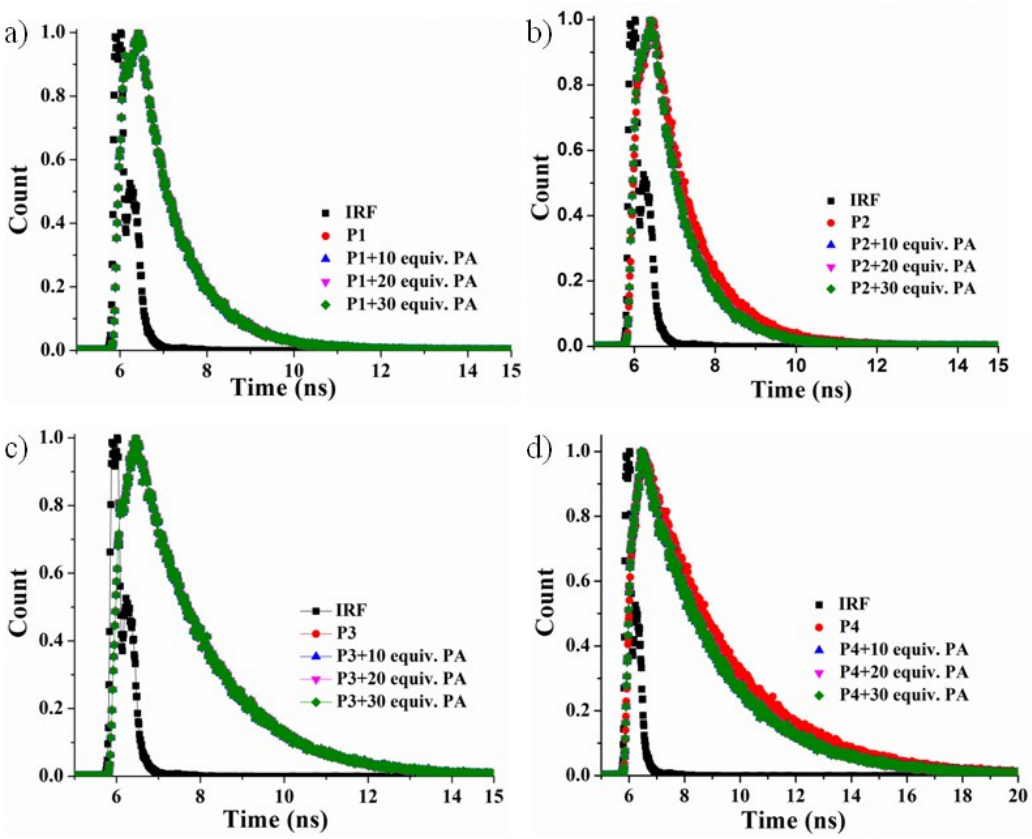

Fig. S36: Time resolved fluorescence spectra of (a) **P1**, (b) **P2**, (c) **P3** and (d) **P4** in presence and absence of PA.

3l. Preparation of thin film and solid state PL measurement

The quartz plates (17 x 15 x 1 mm^3) were cleaned in a fresh piranha solution (7:3 mixture of 98% H_2SO_4 and 30% H_2O_2), washed with Milli-Q water, and followed by ultrasonication in alkaline isopropanol and 0.1 M aqueous HCl at 60 ^oC for 1 h each. After 3 careful washing with Milli-Q water, thin film of the sensing probes (**P1**-**P4**) were prepared by spin coating on quartz plate. A solution of the sensing probe in chloroform (~3 x 10^{-4}M) was dropped on quartz plate and it was spin coated at 1000 rpm for 60 second followed by 1500 rpm for 120 seconds. PL data of the film was measured. After that the film was dipped in different concentration of aqueous picric acid solution for 10 min followed by repetitive and extensive washing by Milli-Q water to remove any unbound (free) picric acid. After drying in air, PL response was recorded.

For the vapour phase study, the thin film was exposed to the picric acid vapour at room temperature. The PL spectra were recorded with different time interval after exposing the thin film to the picric acid vapour. For the film repeatability measurement the thin film was exposed to picric acid vapour for 300 sec and the emission spectrum was recorded. After the each measurement the film was washed with ethanol: water mixture and dried under hot air and the emission spectra was recorded again and the whole process was repeated again for the repeatability test.

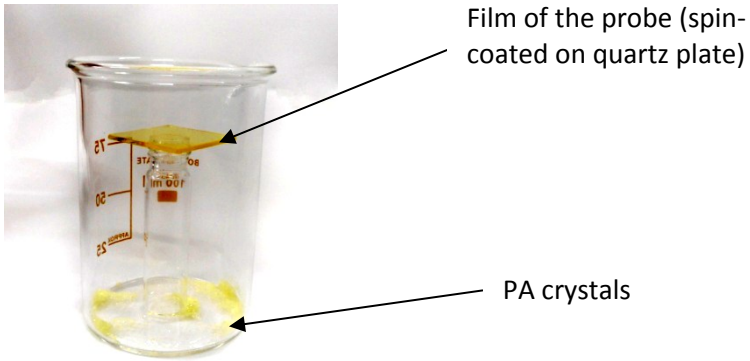

Fig. S37: Experimental set up for demonstrating sensing of PA vapour.

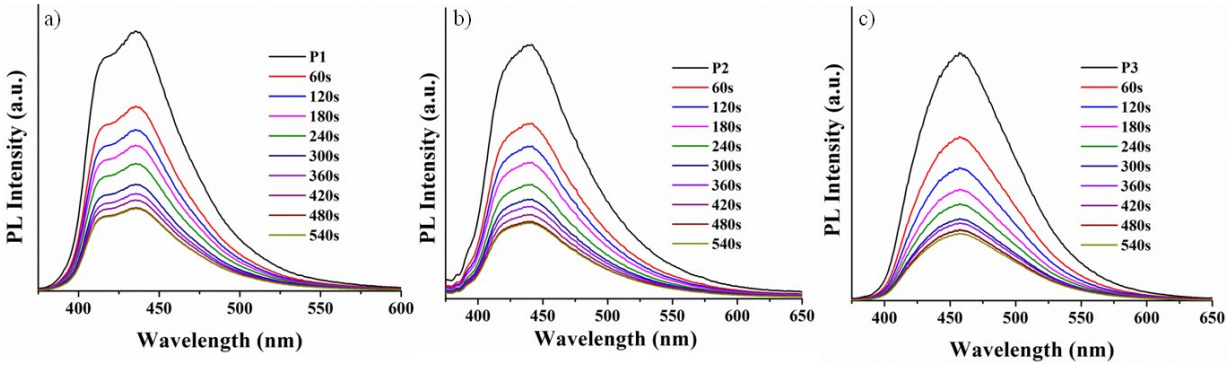

Fig. S38: Emission spectra of (a) **P1**, (b) **P2** and (c) **P3** (as thin film) after exposing with PA vapour varying exposure time.

3m. Repeatability study

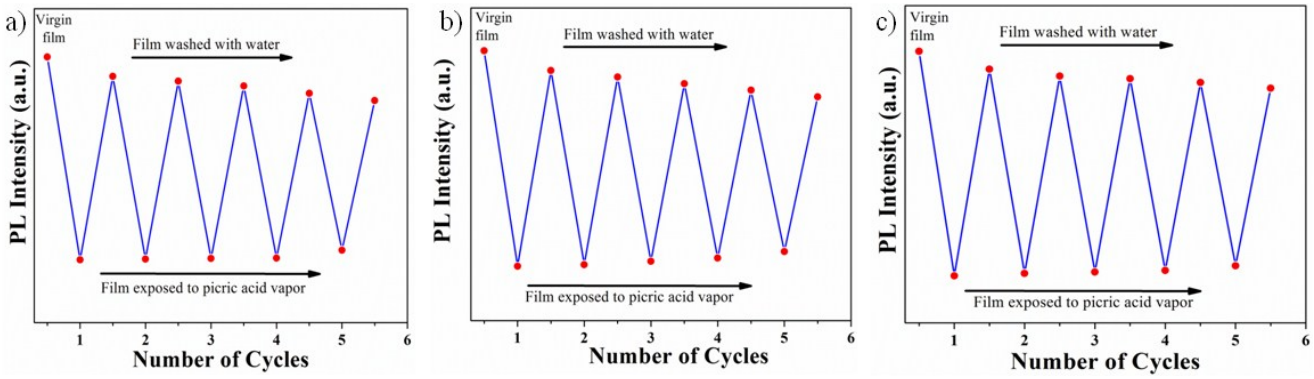

Fig. S39: Repeatability test of (a) **P1**, (b) **P2** and (c) **P3** (as thin film) after exposing with PA vapour.

3n. Changes in emission spectra of the probes (as thin film) towards PA solution:

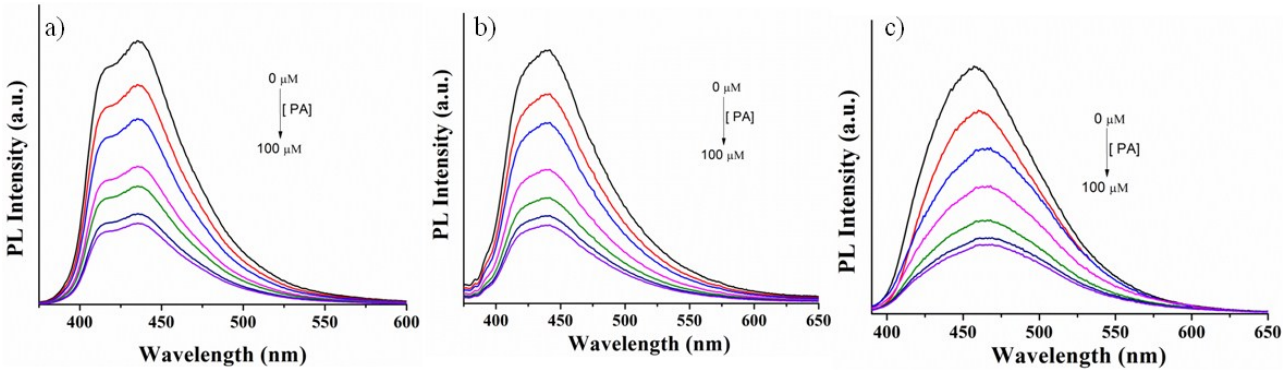

Fig. S40: Emission spectra of (a) **P1**, (b) **P2** and (c) **P3** (as thin film) after exposing with PA solution by varying the concentrations.

3o. Contact-mode detection

For contact-mode sensing, Whatman-42 filter paper was cut into small pieces and dipped into concentrated DCM solution of the sensing probes and subsequently dried in air. PA solution of different concentration (10^{-3} – 10^{-9} M) were prepared and 10μL of each solution was drop-casted on each fresh filter paper strip. When the strips were illuminated under UV at 365 nm, dark spots were observed for PA. The spots were prominent for concentrated sample and slowly faded upon dilution which can be detected by naked eye.

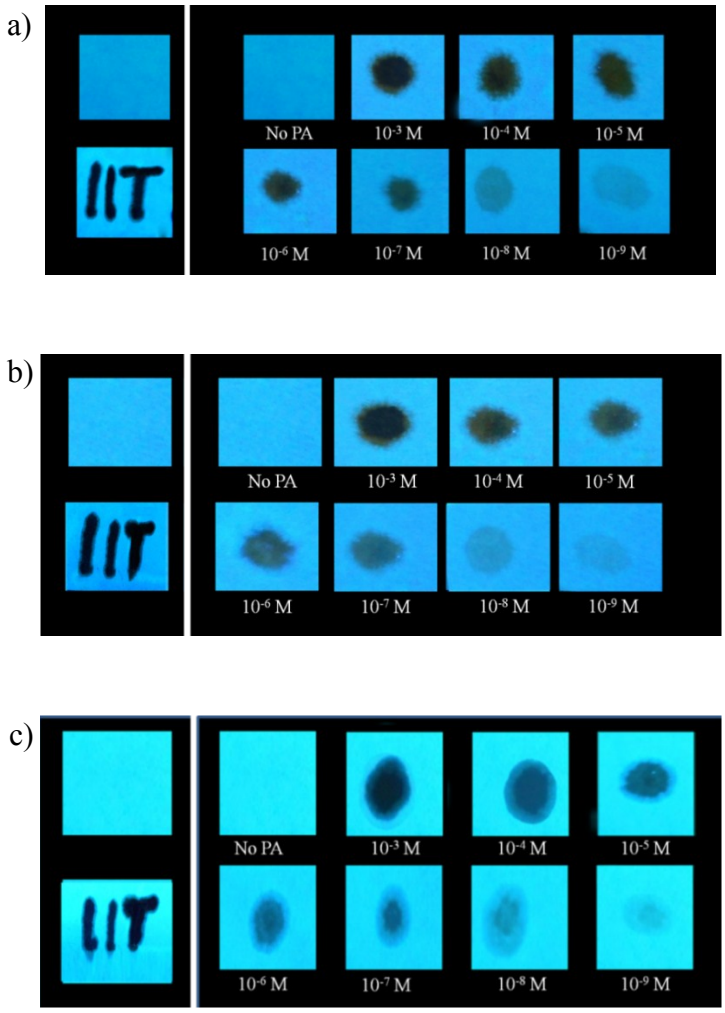

Fig. S41: Visual appearance of (a) **P1**, (b) **P2** and (c) **P3** coated on filter paper before and after the drop casting of different concentrations of PA by contact mode method under the UV illumination at 365nm.

3P. Visual appearance of the probes in absence and presence of PA

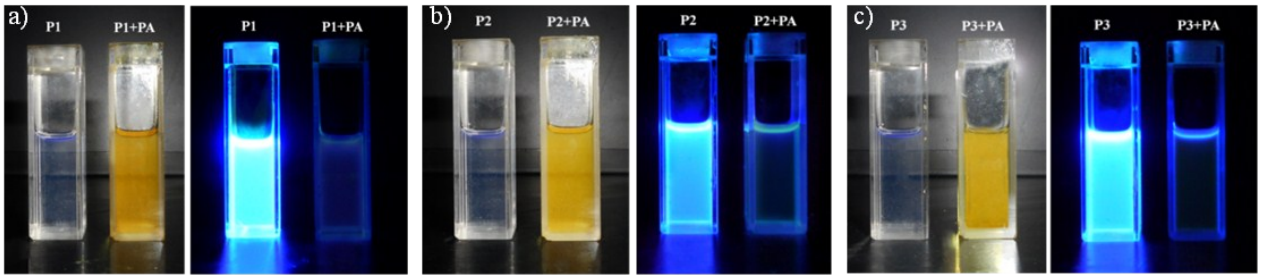

Fig. S42: Visual appearance of (a) **P1**, (b) **P2** and (c) **P3** before and after the addition of PA (Left) under ambient light, (Right) under UV illumination at 365 nm.

4. ^{1}H NMR titration response of the probes towards PA

To investigate the mode of supramolecular interaction between the π-conjugated luminescent arylene-vinylene conjugated terpyridines and NACs, ^{1}H NMR spectroscopic titration studies were carried out with incremental addition of picric acid (PA).

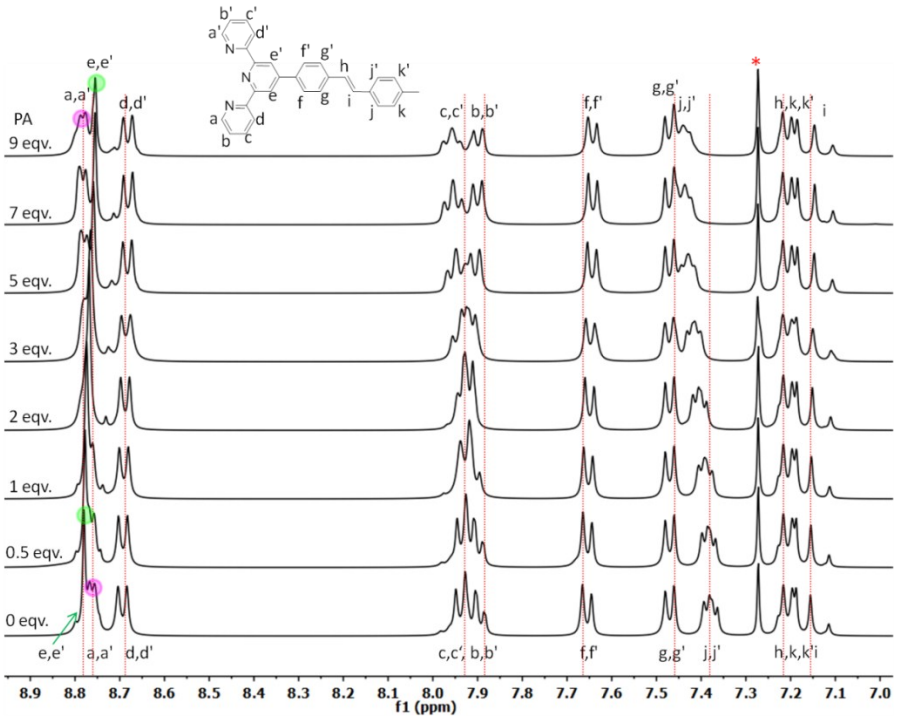

Fig. S43: Chemical shift change of **P1** probe during ^{1}H NMR titration in $CDCl_3$ after incremental addition of PA (* = residual $CHCl_3$).

Table S3. Chemical shift change during ^{1}H NMR titration of probe **P1** with change in concentration of PA

Protons	Chemical shift (ppm)		
	P1	**P1** + PA	Nature of chemical shift
$H_{a,a'}$	8.74	8.77	Down field shift
$H_{c,c'}$	7.91	7.94	
$H_{b,b'}$	7.87	7.89	
$H_{j,j'}$	7.37	7.42	
$H_{e,e'}$	8.76	8.74	Up field shift
$H_{d,d'}$	8.68	8.66	
$H_{f,f'}$	7.65	7.64	
H_h	7.19	7.18	
H_i	7.15	7.13	

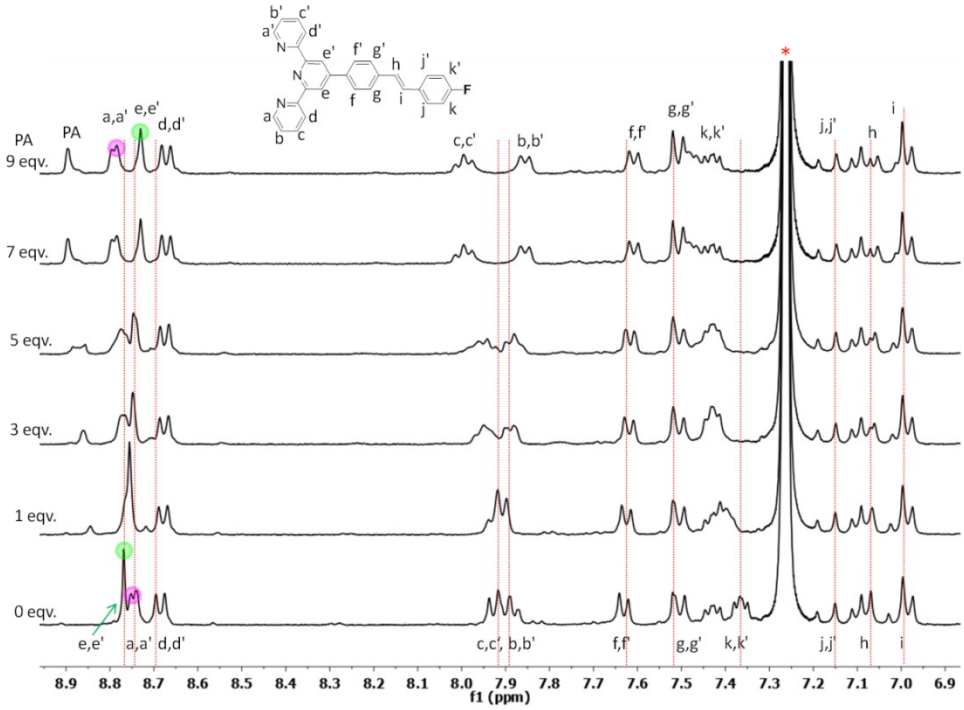

Fig. S44: Chemical shift change of **P2** probe during ^{1}H NMR titration in $CDCl_3$ after incremental addition of PA (* = residual $CHCl_3$).

Table S4. Chemical shift change during ^{1}H NMR titration of probe **P2** with change in concentration of PA

Protons	Chemical shift (ppm)		
	P2	**P2** + PA	Nature of chemical shift
$H_{a,a'}$	8.74	8.78	Down field shift
$H_{c,c'}$	7.93	7.99	
$H_{k,k'}$	7.36	7.43	
$H_{e,e'}$	8.76	8.73	Up field shift
$H_{d,d'}$	8.68	8.67	
$H_{b,b'}$	7.88	7.86	
$H_{f,f'}$	7.63	7.60	
H_h	7.06	7.05	

5. Electrochemical Studies

Determination of HOMO and LUMO from CV studies: Cyclic voltammetric analyses were conducted in acetonitrile using n-Bu_4NPF_6 (0.1 M) as supporting electrolytes, Pt wire counter electrode and Ag/AgCl reference electrode. The HOMO energy levels for **P1**-**P4** were estimated by conventional electrochemical studies. The HOMO energy level (E_{HOMO}) was calculated from the onset oxidation potential (E_{ox}^{onset}) using the following equation: $E_{HOMO} = -(E_{ox}^{onset} + 4.71)$ eV, where the energy level was calibrated against the Ag/AgCl couple. The LUMO energy level (E_{LUMO}) was calculated from the E_{HOMO} energy level and its optical band gap following the equation: $E_{LUMO} = (E_{HOMO} + E_g^{opt})$ eV, as there was no prominent reduction process for **P1**–**P4**.

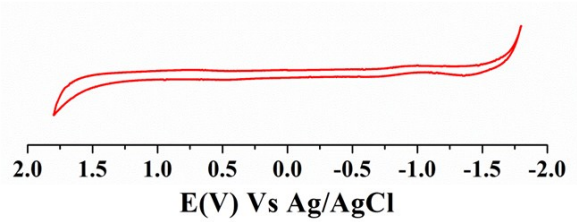

Fig. S45: Cyclic voltammogram of acetonitrile using $TBAPF_6$ as supporting electrolyte (Blank run), Pt disc working electrode, and Ag/AgCl reference electrode. Scan rate at 100mV/s.

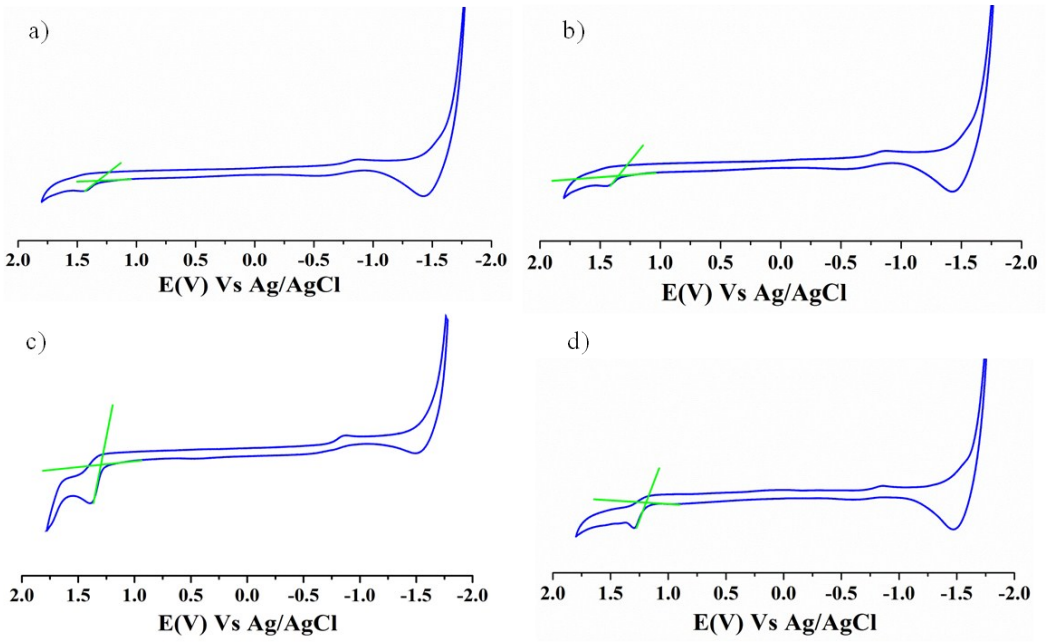

Fig. S46: Cyclic voltammogram of (a) **P1**, (b) **P2**, (c) **P3** and (d) **P4** in acetonitrile using $TBAPF_6$ as supporting electrolyte, Pt disc working electrode, and Ag/AgCl reference electrode. Scan rate at 100 mV/s.

6. FESEM analysis

Preparation of sample for SEM analysis: The sample for FESEM analysis was prepared on a clean 1 cm × 1.5 cm aluminium plate. A solution of the probe in chloroform (~ 5 x 10^{-4} M) was dropped on the alumina substrate, and it was dried under a closed chamber for 2 h. The surface morphology analyses were performed by SEM. The same film was dipped in aqueous solution of picric acid for 5 min followed by repetitive and extensive washing by Milli-Q water to remove the unbound (free) picric acid. The surface morphology was again analyzed.

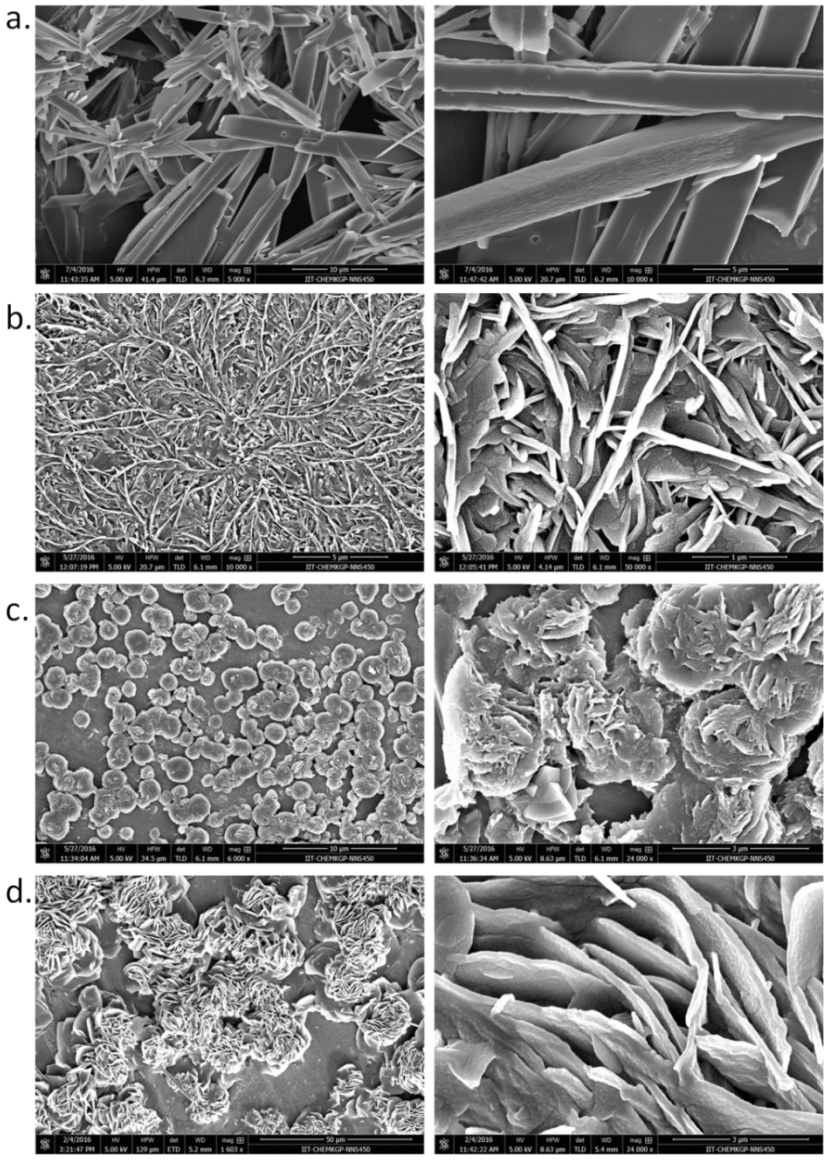

Fig. S47: FESEM images of the sensing probes a) **P1**, b) **P2**, c) **P3**, d) **P4**.

7. Theoretical studies

The geometry optimization of all the arylene-vinyline conjugated terpyridines (**P1**-**P4**) was carried out using density functional theory (DFT) in Gaussian 03 program with B3LYP/6-31g* basis sets.[2] The time dependent density functional theory (TDDFT) calculations have also been performed assuming the solvent as chloroform to predict the energy levels of the HOMO/LUMO. TDDFT calculations were executed at the B3LYP structures using the same basis set as those used in the ground-state DFT calculations. The calculated electronic transitions (major contributions) from TDDFT calculations are provided in Table S8.

Table S5: Computational result of optimized structure of **P1**

Center Number	Atomic Number	Coordinates (Angstroms)		
		X	Y	Z
1	7	5.701199000	-2.206173000	0.959438000
2	6	4.315880000	2.491409000	-0.133535000
3	6	-0.756848000	0.787803000	0.482503000
4	1	-0.294320000	1.610715000	1.020274000
5	6	2.196252000	1.140282000	-0.119656000
6	1	1.629615000	2.056337000	-0.250601000
7	7	4.353112000	0.081141000	0.027379000
8	6	-2.786583000	-0.362292000	-0.223497000
9	7	5.463863000	2.519401000	-0.831252000
10	6	1.535519000	-0.094191000	-0.067741000
11	6	3.596160000	1.182681000	-0.066220000
12	6	4.604504000	-2.316078000	0.190825000
13	6	0.057884000	-0.187750000	-0.121341000
14	6	6.491568000	-3.275250000	1.076062000
15	1	7.368513000	-3.148918000	1.709872000
16	6	6.119906000	3.679187000	-0.907475000
17	1	7.043809000	3.663625000	-1.484415000
18	6	-4.240097000	-0.509034000	-0.309833000
19	1	-4.567989000	-1.378992000	-0.876890000
20	6	3.801263000	3.627659000	0.509751000
21	1	2.885313000	3.561536000	1.088746000
22	6	5.686670000	4.863148000	-0.305673000
23	1	6.266982000	5.775878000	-0.403365000
24	6	4.277169000	-3.502713000	-0.483385000
25	1	3.398246000	-3.547366000	-1.119039000
26	6	2.339276000	-1.237267000	0.034535000
27	1	1.882300000	-2.216634000	0.130795000
28	6	-0.580143000	-1.252033000	-0.778075000
29	1	0.016933000	-2.009153000	-1.278584000

30	6	-6.627150000	0.159003000	0.148721000
31	6	-2.141332000	0.703713000	0.435266000
32	1	-2.728910000	1.475500000	0.923271000
33	6	-8.832283000	1.016092000	0.753310000
34	1	-9.431071000	1.764504000	1.267527000
35	6	-9.469989000	-0.015179000	0.055630000
36	6	3.733959000	-1.106185000	0.074752000
37	6	4.498706000	4.830203000	0.421183000
38	1	4.124760000	5.721161000	0.918770000
39	6	-1.966842000	-1.333690000	-0.828705000
40	1	-2.432743000	-2.164260000	-1.353975000
41	6	-7.442564000	1.101305000	0.799663000
42	1	-6.974994000	1.915450000	1.349173000
43	6	6.248722000	-4.499039000	0.447572000
44	1	6.931974000	-5.332616000	0.580527000
45	6	-5.172589000	0.302261000	0.232522000
46	1	-4.842920000	1.167944000	0.805585000
47	6	5.113054000	-4.609142000	-0.351683000
48	1	4.885332000	-5.535802000	-0.871978000
49	6	-8.659461000	-0.957104000	-0.599612000
50	1	-9.127232000	-1.767310000	-1.155254000
51	6	-7.273969000	-0.876324000	-0.556326000
52	1	-6.687420000	-1.624982000	-1.080825000
53	6	-10.975180000	-0.127960000	0.017781000
54	1	-11.337660000	-0.331122000	-0.996776000
55	1	-11.330197000	-0.948663000	0.655355000
56	1	-11.454318000	0.791487000	0.368958000

Table S6: Computational result of optimized structure of **P2**

Center Number	**Atomic Number**	**Coordinates (Angstroms)**		
		X	**Y**	**Z**
1	7	5.685706000	-2.203215000	0.962295000
2	6	4.298855000	2.492752000	-0.134514000
3	6	-0.772659000	0.785091000	0.483066000
4	1	-0.310509000	1.607212000	1.022285000
5	6	2.179790000	1.140513000	-0.120444000
6	1	1.612538000	2.056177000	-0.251587000
7	7	4.337055000	0.082600000	0.027396000
8	6	-2.801105000	-0.364825000	-0.225566000
9	7	5.446705000	2.520639000	-0.832380000
10	6	1.520237000	-0.094496000	-0.068656000
11	6	3.579689000	1.183789000	-0.066837000
12	6	4.590326000	-2.314329000	0.192055000

13	6	0.042512000	-0.188902000	-0.122664000
14	6	6.476992000	-3.271477000	1.080133000
15	1	7.352847000	-3.144269000	1.715241000
16	6	6.102540000	3.680501000	-0.909059000
17	1	7.026355000	3.664942000	-1.486103000
18	6	-4.254653000	-0.512343000	-0.312517000
19	1	-4.580943000	-1.380294000	-0.883700000
20	6	3.783941000	3.629002000	0.508403000
21	1	2.868069000	3.562944000	1.087557000
22	6	5.669100000	4.864545000	-0.307502000
23	1	6.249267000	5.777325000	-0.405462000
24	6	4.265027000	-3.501198000	-0.482609000
25	1	3.387072000	-3.546778000	-1.119555000
26	6	2.324264000	-1.237220000	0.033999000
27	1	1.867894000	-2.216883000	0.130211000
28	6	-0.594554000	-1.252247000	-0.781687000
29	1	0.003117000	-2.007940000	-1.283525000
30	6	-6.642675000	0.151662000	0.148813000
31	6	-2.157086000	0.700428000	0.435272000
32	1	-2.745012000	1.471368000	0.924245000
33	6	-8.846094000	1.011031000	0.777801000
34	1	-9.471387000	1.732950000	1.292692000
35	6	-9.434298000	-0.021290000	0.058303000
36	6	3.718918000	-1.105187000	0.074944000
37	6	4.481210000	4.831648000	0.419444000
38	1	4.107194000	5.722685000	0.916814000
39	6	-1.981254000	-1.334663000	-0.832680000
40	1	-2.446497000	-2.164517000	-1.359653000
41	6	-7.456106000	1.087778000	0.815884000
42	1	-6.986111000	1.891957000	1.376608000
43	6	6.236309000	-4.495463000	0.451140000
44	1	6.920262000	-5.328306000	0.584972000
45	6	-5.187605000	0.295028000	0.234052000
46	1	-4.858805000	1.157063000	0.812662000
47	6	5.101947000	-4.606755000	-0.349777000
48	1	4.876019000	-5.533612000	-0.870480000
49	6	-8.671305000	-0.969454000	-0.618319000
50	1	-9.168575000	-1.760033000	-1.170839000
51	6	-7.285258000	-0.877441000	-0.569623000
52	1	-6.696329000	-1.618107000	-1.101499000
53	9	-10.779418000	-0.109212000	0.011423000

Table S7: Computational result of optimized structure of **P3**

Center Number	Atomic Number	Coordinates (Angstroms) X	Y	Z
1	7	6.508627000	-1.902435000	0.820276000
2	6	4.602209000	2.650407000	-0.052687000
3	6	-0.240662000	0.389562000	0.611229000
4	1	0.149762000	1.224742000	1.186059000
5	6	2.638250000	1.080656000	-0.048970000
6	1	1.973613000	1.934197000	-0.132564000
7	7	4.897765000	0.253748000	0.012285000
8	6	-2.158214000	-0.924780000	-0.118820000
9	7	5.724817000	2.825351000	-0.770081000
10	6	2.114407000	-0.218502000	-0.032296000
11	6	4.026571000	1.270955000	-0.022668000
12	6	5.407693000	-2.106460000	0.077430000
13	6	0.653483000	-0.464990000	-0.059757000
14	6	7.412536000	-2.882529000	0.879484000
15	1	8.289331000	-2.681648000	1.493943000
16	6	6.254552000	4.049593000	-0.812169000
17	1	7.161757000	4.152863000	-1.406299000
18	6	-3.593523000	-1.204051000	-0.197308000
19	1	-3.848473000	-2.139582000	-0.693943000
20	6	3.986294000	3.701235000	0.644449000
21	1	3.095740000	3.517926000	1.237662000
22	6	5.713894000	5.157941000	-0.155719000
23	1	6.193544000	6.129619000	-0.227349000
24	6	5.189713000	-3.300052000	-0.627971000
25	1	4.302209000	-3.419954000	-1.241548000
26	6	3.036446000	-1.272395000	0.008355000
27	1	2.687764000	-2.297805000	0.074459000
28	6	0.112794000	-1.558994000	-0.753806000
29	1	0.772437000	-2.226621000	-1.300977000
30	6	-1.609985000	0.163428000	0.588695000
31	1	-2.261044000	0.832566000	1.143462000
32	6	4.410096000	-0.994112000	0.025746000
33	6	4.552483000	4.972862000	0.590932000
34	1	4.099039000	5.800158000	1.130578000
35	6	-1.259360000	-1.780929000	-0.781972000
36	1	-1.651212000	-2.628153000	-1.339991000
37	6	7.283932000	-4.105285000	0.216133000
38	1	8.056499000	-4.863615000	0.302364000
39	6	-4.599707000	-0.419484000	0.242677000
40	1	-4.354614000	0.545874000	0.679201000
41	6	6.143351000	-4.312881000	-0.556250000
42	1	6.001150000	-5.242040000	-1.101847000
43	6	-6.026810000	-0.761368000	0.183672000

44	6	-7.027375000	0.266811000	0.043911000
45	6	-6.440170000	-2.083500000	0.291258000
46	6	-6.707902000	1.644520000	-0.103818000
47	6	-8.413853000	-0.105471000	0.029641000
48	6	-7.802923000	-2.443230000	0.256612000
49	1	-5.694672000	-2.858556000	0.442121000
50	6	-7.692883000	2.600383000	-0.226077000
51	1	-5.668478000	1.952857000	-0.138880000
52	6	-9.404911000	0.904898000	-0.098715000
53	6	-8.772764000	-1.474910000	0.134686000
54	1	-8.080986000	-3.489689000	0.347909000
55	6	-9.057605000	2.230412000	-0.218937000
56	1	-10.450722000	0.606509000	-0.103530000
57	1	-9.826371000	-1.743293000	0.122487000
58	1	-9.826093000	2.992377000	-0.316097000
59	1	-7.418980000	3.646192000	-0.336407000

Table S8: Computational result of optimized structure of **P4**

Center Number	**Atomic Number**	**Coordinates (Angstroms)**		
		X	**Y**	**Z**
1	7	-7.026120000	-2.074044000	1.025473000
2	6	-5.501061000	2.502257000	-0.366875000
3	6	-0.485330000	0.572144000	-0.723959000
4	1	-0.949440000	1.252204000	-1.432769000
5	6	-3.409742000	1.127479000	-0.132579000
6	1	-2.820285000	2.029787000	-0.257764000
7	7	-5.589236000	0.113049000	-0.016087000
8	6	1.540934000	-0.426493000	0.188084000
9	7	-6.607873000	2.493659000	-1.128578000
10	6	-2.775281000	-0.105307000	0.066304000
11	6	-4.809278000	1.192412000	-0.163150000
12	6	-5.891373000	-2.258977000	0.330155000
13	6	-1.297867000	-0.218409000	0.109388000
14	6	-7.841171000	-3.119645000	1.179698000
15	1	-8.748908000	-2.932118000	1.751993000
16	6	-7.240227000	3.652825000	-1.323369000
17	1	-8.130798000	3.607084000	-1.949033000
18	6	2.997682000	-0.567161000	0.280566000
19	1	3.340855000	-1.411467000	0.876674000
20	6	-5.004112000	3.675181000	0.222184000
21	1	-4.123389000	3.639847000	0.855903000
22	6	-6.822384000	4.871348000	-0.782801000
23	1	-7.382308000	5.781481000	-0.976466000

24	6	-5.549040000	-3.498583000	-0.231862000
25	1	-4.638135000	-3.604807000	-0.812822000
26	6	-3.602541000	-1.224733000	0.222812000
27	1	-3.167402000	-2.206529000	0.377810000
28	6	-0.662272000	-1.121263000	0.976490000
29	1	-1.259307000	-1.731336000	1.648401000
30	6	0.898793000	0.467217000	-0.690984000
31	1	1.488316000	1.071875000	-1.373906000
32	6	-4.994739000	-1.072967000	0.171682000
33	6	-5.676888000	4.876332000	0.010008000
34	1	-5.317254000	5.795933000	0.464124000
35	6	0.724163000	-1.221806000	1.012632000
36	1	1.190890000	-1.919931000	1.703592000
37	6	-7.586770000	-4.391743000	0.661389000
38	1	-8.291501000	-5.202773000	0.819302000
39	6	3.923445000	0.254580000	-0.254767000
40	1	3.582990000	1.143672000	-0.784089000
41	6	-6.411439000	-4.579411000	-0.062553000
42	1	-6.172896000	-5.546607000	-0.497145000
43	6	5.386659000	0.101405000	-0.142773000
44	6	6.040780000	-1.122454000	-0.454500000
45	6	6.154747000	1.228497000	0.261053000
46	6	5.356649000	-2.274058000	-0.963069000
47	6	7.476891000	-1.220231000	-0.304882000
48	6	7.589544000	1.121448000	0.373158000
49	6	6.022057000	-3.439672000	-1.242952000
50	1	4.291771000	-2.209675000	-1.149518000
51	6	8.130413000	-2.459424000	-0.594252000
52	6	8.208803000	-0.102166000	0.102465000
53	6	7.426930000	-3.544496000	-1.040663000
54	1	9.208018000	-2.513929000	-0.458592000
55	1	9.288878000	-0.184696000	0.205659000
56	1	7.936134000	-4.479023000	-1.259725000
57	1	5.473237000	-4.291551000	-1.635611000
58	6	8.348595000	2.263931000	0.775842000
59	1	9.428884000	2.163102000	0.849565000
60	6	7.736952000	3.454052000	1.065243000
61	1	8.325152000	4.315408000	1.369579000
62	6	6.320682000	3.560216000	0.980831000
63	1	5.838893000	4.501762000	1.230488000
64	6	5.558680000	2.484535000	0.601358000
65	1	4.478903000	2.582476000	0.576585000

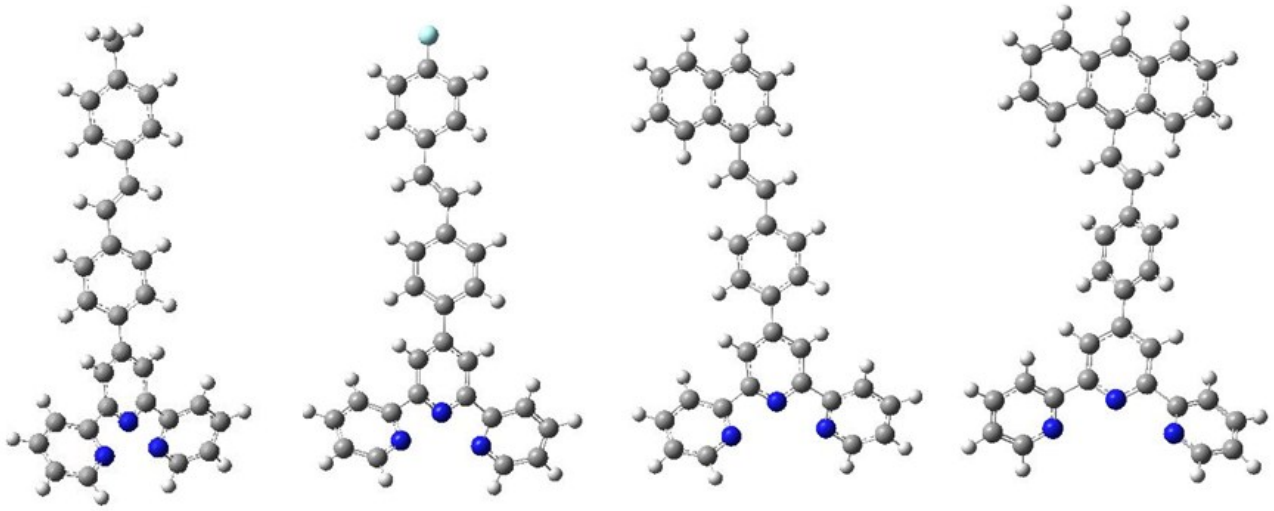

Fig. S48: Optimized geometric conformations of **P1** - **P4** (from left to right)

Table S8: Electronic transitions calculated by TDDFT method for the probes.

Probes	$E_{excitation}$ (eV)	$\lambda_{excitation}$ (nm)	Osc. Strength (f)	Key transitions
P1	3.5103	353.20	1.2734	HOMO→LUMO
P2	3.4208	362.44	1.5596	HOMO→LUMO
	4.1573	298.23	0.1917	HOMO→LUMO+2
	4.7873	258.99	0.2047	HOMO-1→LUMO+2
P3	3.2834	377.61	1.1893	HOMO→LUMO
	4.1271	300.42	0.1726	HOMO→LUMO+3
	4.4183	280.62	0.1963	HOMO→LUMO+2
P4	3.2690	379.27	0.938	HOMO→LUMO HOMO→LUMO+1
	3.4206	362.47	0.1483	HOMO→LUMO+2
	3.9830	311.28	0.3956	HOMO-1→LUMO HOMO-1→LUMO+1
	4.0502	306.12	0.3444	HOMO-1→LUMO+1
	4.1521	298.61	0.1535	HOMO-2→LUMO+1 HOMO-1→LUMO+3
	4.7525	260.88	0.3299	HOMO-2→LUMO+1 HOMO-2→LUMO+3

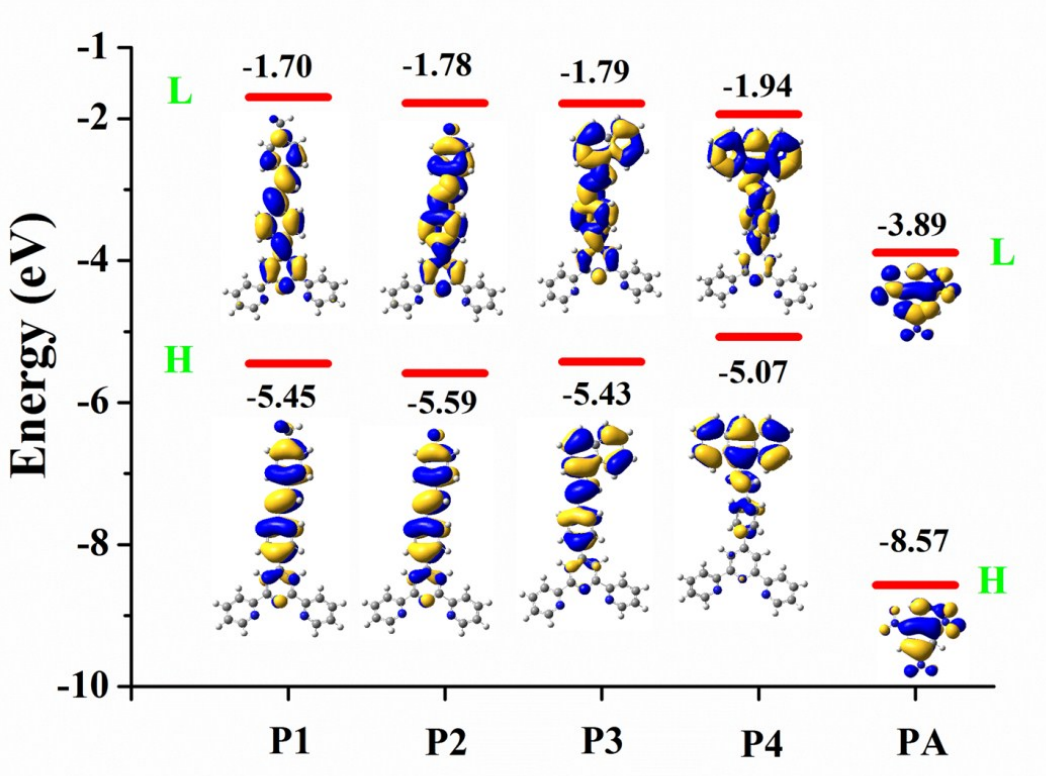

Fig. S49: Energy level diagram of the frontier molecular orbitals of the probes (**P1**-**P4**) calculated using TDDFT theory at B3LYP level; L = LUMO energy level and H= HOMO energy level.

8. References

S1. (a) J. R. Lakowicz, Principles of Fluorescence Spectroscopy; Plenum: New York, 1999; Vol. (b) A. Chakraborty, D. Chakrabarty, P. Hazra, D. Seth and N. Sarkar, Chem. Phys. Lett., 2003, **382**, 508.

S2. Gaussian 03, Revision C.02, M. J. Frisch, G. W. Trucks, H. B. Schlegel, G. E. Scuseria, M. A. Robb, J. R. Cheeseman, J. A. Montgomery, Jr., T. Vreven, K. N. Kudin, J. C. Burant, J. M. Millam, S. S. Iyengar, J. Tomasi, V. Barone, B. Mennucci, M. Cossi, G. Scalmani, N. Rega, G. A. Petersson, H. Nakatsuji, M. Hada, M. Ehara, K. Toyota, R. Fukuda, J. Hasegawa, M. Ishida, T. Nakajima, Y. Honda, O. Kitao, H. Nakai, M. Klene, X. Li, J. E. Knox, H. P. Hratchian, J. B. Cross, V. Bakken, C. Adamo, J. Jaramillo, R. Gomperts, R. E. Stratmann, O. Yazyev, A. J. Austin, R. Cammi, C. Pomelli, J. W. Ochterski, P. Y. Ayala, K. Morokuma, G. A. Voth, P. Salvador, J. J. Dannenberg, V. G. Zakrzewski, S. Dapprich, A. D. Daniels, M. C. Strain, O. Farkas, D. K. Malick, A. D. Rabuck, K. Raghavachari, J. B. Foresman, J. V. Ortiz, Q. Cui, A. G. Baboul, S. Clifford, J. Cioslowski, B. B. Stefanov, G. Liu, A. Liashenko, P. Piskorz, I. Komaromi, R. L. Martin, D. J. Fox, T. Keith, M. A. Al-Laham, C. Y. Peng, A. Nanayakkara, M. Challacombe, P. M. W. Gill, B. Johnson, W. Chen, M. W. Wong, C. Gonzalez, J. A. Pople, Gaussian, Inc., Wallingford CT, 2004.